HHS Public Access

Author manuscript

Dev Biol. Author manuscript; available in PMC 2021 August 01.

Published in final edited form as:

Dev Biol. 2020 August 01; 464(1): 53–70. doi:10.1016/j.ydbio.2020.05.002.

Mask, a component of the Hippo Pathway, is required for *Drosophila* eye morphogenesis.

Miles W DeAngelis, **Emily W McGhie**, **Joseph D Coolon**, **Ruth I Johnson**[1]

Wesleyan University Department of Biology, Middletown CT, 06457

Abstract

Hippo signaling is an important regulator of tissue size, but it also has a lesser-known role in tissue morphogenesis. Here we use the *Drosophila* pupal eye to explore the role of the Hippo effector Yki and its cofactor Mask in morphogenesis. We found that Mask is required for the correct distribution and accumulation of adherens junctions and appropriate organization of the cytoskeleton. Accordingly, disrupting *mask* expression led to severe mis-patterning and similar defects were observed when *yki* was reduced or in response to ectopic *wts*. Further, the patterning defects generated by reducing *mask* expression were modified by Hippo pathway activity. RNA-sequencing revealed a requirement for Mask for appropriate expression of numerous genes during eye morphogenesis. These included genes implicated in cell adhesion and cytoskeletal organization, a comprehensive set of genes that promote cell survival, and numerous signal transduction genes. To validate our transcriptome analyses, we then considered two loci that were modified by Mask activity: *FER* and *Vinc*, which have established roles in regulating adhesion. Modulating the expression of either locus modified *mask* mis-patterning and adhesion phenotypes. Further, expression of *FER* and *Vinc* was modified by Yki. It is well-established that the Hippo pathway is responsive to changes in cell adhesion and the cytoskeleton, but our data indicate that Hippo signaling also regulates these structures.

Graphical Abstract

[1]Corresponding Author: Ruth I Johnson: rijohnson@wesleyan.edu.

Co-authors:

Miles W DeAngelis

Emily W McGhie

Joseph D Coolon

AUTHOR CONTRIBUTIONS

Conceptualization, M.W.D. and R.I.J.; Methodology, M.W.D., J.D.C. and R.I.J.; Validation, M.W.D., E.W.M, J.D.C. and R.I.J.; Investigation, M.W.D., E.W.M, and R.I.J.; Data Curation, M.W.D., J.D.C. and R.I.J.; Writing – original draft, M.W.D. and R.I.J.; Writing – review & editing, M.W.D., E.W.M, J.D.C. and R.I.J.; Visualization, M.W.D., J.D.C. and R.I.J.; Supervision - J.D.C. and R.I.J.; Project Administration, R.I.J.; Funding Acquisition – R.I.J.

DECLARATION OF INTERESTS

The authors declare no competing interests

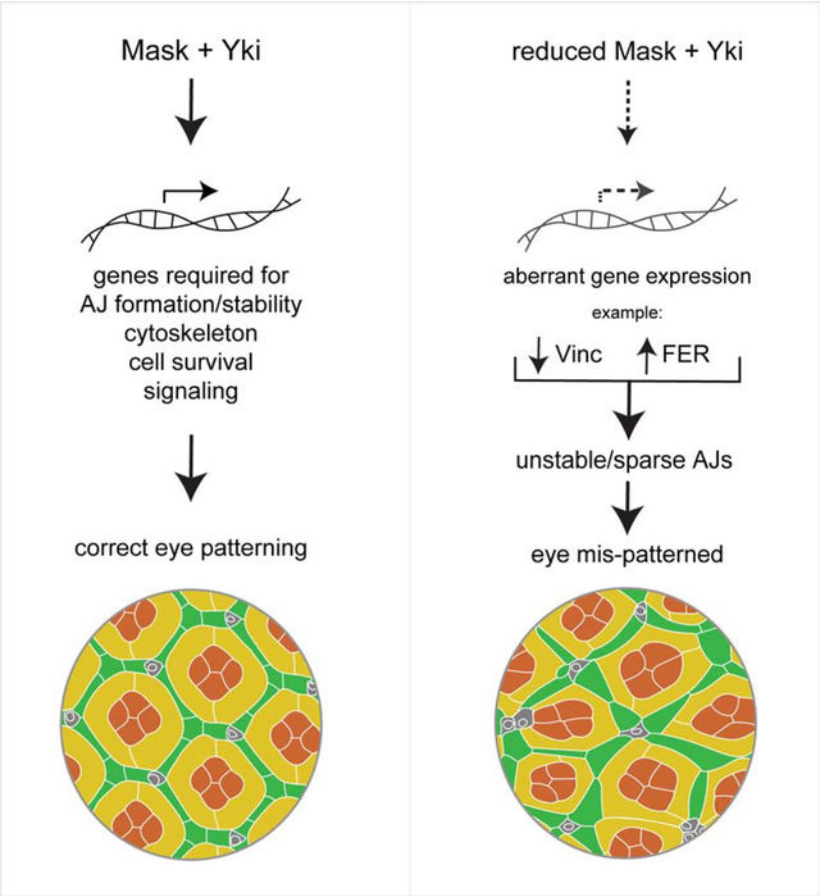

Keywords

morphogenesis; *Drosophila*; eye; Hippo; Yorkie; Mask

INTRODUCTION

Since the final structure of any cell in a tissue is the outcome of the mechanical constraints and forces placed on that cell, adhesive junctions established with its neighbors, and the structure of the cell's internal cytoskeleton, understanding the mechanisms that regulate these elements in a developing or mature tissue is important. Recently, a number of studies in vertebrates have suggested that Hippo signaling can modify or respond to these aspects of cell anatomy and is therefore important in tissue and organ morphogenesis (Zheng and Pan, 2019). However, since the pre-dominant role for Hippo signaling is regulation of cell proliferation and survival (Boopathy and Hong, 2019; Misra and Irvine, 2018; Watt et al., 2017), clarifying the contribution of Hippo to tissue morphogenesis is challenging. To circumvent this issue we utilize the *Drosophila* pupal eye as a model since it is post-mitotic and, in addition, becomes refractive to apoptosis (Cagan and Ready, 1989b; Wolff and Ready, 1991a; Wolff and Ready, 1991b). Hence, in the fly eye we can examine more precisely the role of Hippo signaling in morphogenesis, independent of its function in tissue growth.

The Hippo pathway negatively regulates the transcriptional coactivator Yorkie (Yki, YAP/TAZ in mammals) (Dong et al., 2007; Huang et al., 2005; Lei et al., 2008; Zhao et al., 2007). When active, Yki translocates to the nucleus to facilitate transcription of genes that regulate cell division or apoptosis including: *Cyclin E*, *Diap1* and *bantam* (Peng et al., 2009; Tapon et al., 2002; Wu et al., 2003). Yki does not contain a DNA binding domain but instead influences gene expression via interactions with transcription factors including *scalloped* (*sd*), *homothorax* (*hth*), *teashirt* (*tsh*) and *Mothers against decapentaplegic* (*Mad*) (Goulev et al., 2008; Oh and Irvine, 2011; Peng et al., 2009; Staley and Irvine, 2012; Wu et al., 2008). Due to the proliferative consequence of Yki activity, its appropriate cellular regulation is essential and this is predominantly achieved via phosphorylation by Warts (Wts), which in turn is activated by Hippo (Hpo) (Harvey et al., 2003). Phosphorylated Yki is bound by cytoplasmic 14-3-3 and consequently sequestered from the nucleus (Dong et al., 2007; Ren et al., 2010b).

Mask (multiple ankyrin repeats single KH domain) is a 423 kDa protein that contains two ankyrin repeat domains (suggesting a scaffolding role) and a single K-homology domain (that may mediate interactions with nucleic acids) that was first identified during a screen for novel receptor tyrosine kinase (RTK) signaling components (Smith et al., 2002). Mask has two mammalian orthologues - Mask1 and Mask2 - and recent studies indicate that Mask family proteins regulate the import of Yki/YAP into the nucleus and are therefore required for their full transcriptional activity (Kwon et al., 2013; Li et al., 2017; Machado-Neto et al., 2014; Sansores-Garcia et al., 2013; Sidor et al., 2019; Sidor et al., 2013). Hence Mask is described as a Yki/YAP cofactor.

Studies that implicate Hippo signaling in tissue morphogenesis have mainly considered this role in vertebrates. For example, YAP is required for nephron development in the mammalian kidney (McNeill and Reginensi, 2017; Reginensi et al., 2016; Reginensi et al., 2013) and urinary tract morphogenesis (Reginensi et al., 2015). YAP also contributes to lung development where it promotes gene expression that is associated with myosin II activation and the generation of tensile forces necessary for branching morphogenesis (Lin et al., 2017). YAP also promotes transcription of genes associated with increased cellular tension in hepatocytes, which correlates with antagonism of adherens junction (AJ) formation (Bai et al., 2016). In contrast, YAP is required for VE-cadherin distribution and correct adhesion during angiogenesis in the mouse brain and retina (Kim et al., 2017a). Hence, mounting evidence indicates that cytoskeletal and junction structures are modified via YAP-mediated transcription in developing tissues and these effects are likely to extend to cancer as well. Indeed, in cancer-associated fibroblasts, ectopic YAP has been shown to modulate the expression of genes that modify actin and myosin structures to promote cell migration (Calvo et al., 2013). Mask1 has similarly been implicated as a regulator of cancer cell migration. For example, reduced expression of *mask1* decreased the migration of multiple myeloma cells, hepatocellular carcinoma cells, and colorectal cancer cells in which YAP activity was associated with the transcription of genes that promote epithelial to mesenchymal transition (Dhyani et al., 2015; Yao et al., 2018; Zhou et al., 2019).

The effects of YAP and Mask1 in modifying junction/cytoskeletal structures are suggestive of a feedback loop since these structures are also well-documented modifiers of Hippo

signaling. For example, activity of the core AJ components E-cadherin (E-cad) and α-catenin (α-cat) has been linked to activation of the core Hippo kinase LATS1/2 and inhibition of YAP (Kim et al., 2011; Schlegelmilch et al., 2011; Silvis et al., 2011), and in *Drosophila* the Ig-CAM protein Echinoid that localizes to AJs can promote Salvador/Hpo activity to inhibit Yki (Yue et al., 2012). A complex picture of cytoskeletal regulation of Hippo signaling, mainly via interactions with Wts/LATS or Hpo/MST, is emerging (Seo and Kim, 2018; Zheng and Pan, 2019). F-actin accumulation, elaboration of branched F-actin networks and activation of contractile actin-myosin networks have all been shown to increase nuclear Yki/YAP/TAZ activity (Aragona et al., 2013; Dupont et al., 2011; Fernández et al., 2011; Gaspar et al., 2015; Matsui and Lai, 2013; Rauskolb et al., 2014; Sansores-Garcia et al., 2011; Wada et al., 2011; Zhao et al., 2012). Conversely, activity of the spectrin-based membrane skeleton is considered to antagonize Yki/YAP (Deng et al., 2015; Fletcher et al., 2015).

The functions of Hippo pathway proteins, Yki, and its nuclear interactors have been extensively characterized in proliferative *Drosophila* tissues. Here, using the post-mitotic *Drosophila* pupal retina as a model, we found that correct activity of Mask, Yki and Wts is required for the appropriate distribution of AJs and hence eye patterning. In addition, we determined that Mask activity impacts the expression of numerous genes during eye patterning, including many associated with cell adhesion and cytoskeletal organization. Indeed two of these – *FER tyrosine kinase* (antagonized by Mask activity) and *Vinculin* (promoted by Mask) – contributed to the correct organization of AJs and eye patterning. We also found that Mask regulates a large number of genes associated with signal transduction and many genes that modify apoptosis to promote cell survival. These latter data emphasize that an entire gene program, rather than a select few genes, is modified by Hippo signaling to determine whether cells survive or die. Taken together, our data underscore a pivotal role for Hippo in epithelial morphogenesis.

MATERIALS AND METHODS

Fly stocks

The following fly stocks were used (BL-Bloomington Drosophila Stock Center, v-Vienna Drosophila Research Center): w^{1118} (BL-3605), *GMR-Gal4* (BL-1104), *Gal4–54C* (BL-27328), *mirror-Gal4 / TM6b* (BL-29650), *ptc-Gal4* (BL-2017), *GMR-Gal4, UAS-Dcr-2* (Johnson et al., 2011), *UAS-mask*^{RNAi} (v29541-no longer maintained by the VDRC), *UAS-mask*^{RNAi} (v103411), *UAS-mask*^{RNAi} (v33396), *UAS-yki*^{RNAi} (v104524), *UAS-FER*^{dsRNA}; *UAS-FER*^{dsRNA} (BL-9366), *UAS-GFP*^{dsRNA} (BL-9330), *UAS-Ecad*$^{RNAi\ B107A1}$ (Seppa et al., 2008), *mask*^{EY01848} (BL-15378), *UAS-mask*^{RA} (Zhu et al., 2015a), *UAS-2XEGFP*^{AH2} (BL-6874), *UAS-yki*^{V5} (BL-28819), *UAS-FER.p100* (BL-9365), *UAS-shg*^{R5} (BL-58494), *UAS-lacZ* (BL-3955), *UAS-GFP* (BL-4776), *UAS-Diap1* (BL-6657), *UAS-rpr* (BL-5824), *UAS-Vinc RFP* (Maartens et al., 2016), *GMR-wts*$^{A1–1}$ (Tapon et al., 2002), *wts*^{X1}, *FRT82b / TM6b* (BL-44251), *hsFLP*^{12}; *FRT42D, hpo*^{KS240} / *CyO* (BL-25085), *ey-FLP*^{N2}; *FRT42D, hpo*^{KC202} / *CyO, Kr-GFP* (BL-25090), *mer*^{4}, *FRT19A / FM7i, Act-GFP* (BL-9104), *ex*^{e1}, *FRT40A / CyO* (BL-44249), *FER*^{X21} (BL-9362), *mask*$^{5.8}$ / *TM6b* (Smith et al., 2002), *mask*$^{10.22}$ / *TM6b* (Smith et al., 2002), *shg*^{R69};*TM2 / SM5-TM6b* (Godt and Tepass, 1998),

yki^{B5}, *FRT42D / CyO-GFP* (Oh and Irvine, 2008), *Vinc*$^{\Delta 1}$ (Klapholz et al., 2015), *shg-tomato* (BL-58789), *lifeact-GFP* (BL-35544), *sqh-GFP* (BL-57145), *mask*^{CC00924} (BL-51547), *mask*$^{sf\text{-}GFP\text{-}\ TVPTBF}$ (v318123), *yki*$^{sf\text{-}GFP\text{-}\ TVPTBF}$ (v318237), *yki-YFP* (Su et al., 2017). For further information on fly lines, see Table S1.

Dissection and immunofluorescence

All crosses were maintained at 25°C and tissue dissected in PBS and fixed in 4% formaldehyde using standard procedures. For immunohistochemistry, primary antibodies were rat anti-E-cad (1:20, DSHB, #528120), mouse anti-Discs large (Dlg) (1:50, DSHB, #528203), rabbit anti-Dcp-1 (1:100, Cell-Signaling Technology, #9578), rabbit anti-PH3 (1:200, Millipore Sigma, #06–570), chicken anti-GFP (1:20, Abcam, #13970), mouse anti-Lamin DMO (1:10, DSHB, #528336), rabbit anti-Mask (1:500), (Smith et al., 2002), (antibody no longer available). Secondary antibodies (Jackson ImmunoResearch) were conjugated to Alexa Fluor® 488, Cy3 or Alexa Fluor® 647 and used at dilutions of 1:200, 1:100, or 1:50, respectively. For cytoskeletal imaging (Figure S9), pupal eyes were dissected in ice-cold PBS, fixed in 4% formaldehyde with phalloidin (1:500, Thermo Fisher Scientific, #P3457), washed twice in ice-cold PBS and ice-cold PBT, mounted and then imaged.

Microscopy and image processing

Tissue was imaged with a Leica DM5500 B fluorescence microscope, Leica SP8 confocal microscope or Zeiss LSM510 confocal microscope and associated software. Adult eyes were imaged with a Leica M125 stereo-dissected microscope, Leica IC80HD camera and Leica Acquire version 3.3 software at 6.3X magnification. All adult animals shown are female with the exception of Fig. 1K. Confocal microscopy parameters were identical when imaging control and experimental tissues but for images gathered using standard fluorescence microscopy, imaging parameters were optimized for maximal E-cad detection. Image files were processed for publication using Adobe Photoshop. All images presented are of tissue in the center of retinas. Image tracings were drawn in Adobe Illustrator.

Analysis of density and distribution of E-cadherin at AJs, and retinal mis-patterning

Retinas of different genotypes were prepared and imaged in parallel, with identical conditions. Three independent replicates of each experiment were performed. Maximum projection images spanning the AJs were assembled from confocal Z-stacks and imported into ImageJ and pixel intensity of junctions between lattice and 1° cells located in the center of retinas was determined. Junctions were randomly selected for these analyses. Normalized junctional intensity was calculated as (average pixel intensity of cell junction) - (background pixel intensity), where the latter value was determined as an average of the pixel intensity of the apical cytoplasm in the center of both neighboring cells. For quantification of the distribution of E-cad along at AJs (coverage, %), maximum projection image files were imported into ImageJ and a) the length of randomly-selected AJs between lattice and 1° cells in the center of retinas measured, and b) gaps in E-cad distribution along the AJ measured. Gaps were identified as regions of the AJ with no detected fluorescence (pixel intensity = 0). E-cad coverage (%) was the defined as (1-(sum of all gap lengths/total AJ length))x100. To generate mean ommatidial mis-patterning scores (OMS) a hexagonal grid was superimposed over images of the central region of retinas, as previously described (Johnson and Cagan,

2009). Each hexagon was drawn so that the centers of 6 ommatidia surrounding a central ommatidium were connected. Ommatidia and the surrounding lattice cells and bristle groups within each drawn hexagon (or data point) were scored for defects to generate an OMS. Cone cells defects scored included changes in cell number, orientation, and failure to establish correct contacts between cells. For 1° pigment cells, defects scored included changes in 1° cell number, unequal 1° cell size, failure to establish the 1°-1° cell junction and resulting contacts between cone cells and lattice cells or bristle groups as a result. For 2° and 3° cells (lattice cells) defects scored included changes in lattice cell number and failure to correctly establish the 3° niche. For bristle groups, changes in the number and position of bristle groups were scored. For all analyses, statistical significance was determined using One-Way Analysis of Variance (ANOVA).

qRT-PCR and RNA-sequencing

mRNA was prepared, in triplicate, from *GMR>lacZ*; *GMR>GFP^{RNAi}*; *GMR>mask$^{RNAi\ v29541}$*; *GMR>GFP^{RNAi}*, *Dcr-2*; and *GMR>yki^{RNAi}*, *Dcr-2* retinas using either standard Trizol extraction and reverse transcriptase (Invitrogen, #18090010) or the ReliaPrep RNA Tissue Miniprep System (Promega Corporation, # M3001), as previously described (DeAngelis and Johnson, 2019). Duplicate qRT-PCR analyses were performed using a Step One Plus Real-Time PCR System (Applied Biosystems, # 4376600) with primer sets listed in Table S2. For each gene assayed with qRT-PCR, expression was quantified by determining the threshold cycle for each reaction (C_T) and C_T values compared to the housekeeping gene *rp49* to generate estimates of relative expression (ΔC_T). Replicate ΔC_T values were then compared to generate estimates of differential expression ($\Delta\Delta C_T$). Specificity of amplified products generated was confirmed with melt curve analysis and gel electrophoresis. Significant changes in gene expression were determined with two-sample two-sided student's t-tests.

The *UAS-mask$^{RNAi\text{-}v29541}$*, *UAS-GFP^{RNAi}*, *UAS-GFP*, *mask^{EY01848}* and *GMR-Gal4* lines were isogenized by backcrossing to *w^{1118}* for five generations and then rebalanced. mRNA was isolated in triplicate from 50–70 retinas of *GMR>GFP^{RNAi}* and *GMR>mask$^{RNAi\text{-}v29541}$*; and *GMR>GFP and GMR>mask^{EY01848}* as described (DeAngelis and Johnson, 2019). *GMR>GFP^{RNAi}* and *GMR>mask$^{RNAi\text{-}v29541}$* replicates were dissected on different days than *GMR>GFP and GMR>mask^{EY01848}* replicates. Barcoded cDNA library preparation was performed using TruSeq library preparation kits, libraries were pooled and balanced pooling was confirmed using qPCR and paired-end 51bp RNA-sequencing were all performed by the University of Michigan Advanced Genomics and Next Generation Sequencing Core. Sequencing reads were imported into Galaxy (https://usegalaxy.org/) and their quality assessed with FASTQC (Afgan et al., 2018; Andrews, 2010). Bioinformatics processing of sequence data followed the approach of (Lanno et al., 2017). Briefly, sequence reads were aligned to the *D. melanogaster* reference genome and gene annotation files available at the time of submission (reference genome: Drosophila_melanogaster.BDGP6.dna.toplevel.fa, gene annotation: Drosophila_melanogaster.BDGP6.93.gff3) downloaded from Ensembl (Zerbino et al., 2018) with Bowtie2 (Langmead and Salzberg, 2012) using default parameters. The percentage of mapped reads was determined with Flagstat from SAMtools (Li et al., 2009). Gene

expression quantification and differential gene expression statistical analyses were performed using Cuffdiff following geometric normalization and transcript length correction where bias correction was performed using the reference genome sequence (Trapnell et al., 2012). Sequencing reads mapping to the *UAS-mask*$^{RNAi\text{-}v29541}$ transgene were quantified, to confirm *mask* reduction, using cufflinks (Trapnell et al., 2010). Statistical comparisons of *mask* long isoform expression to corresponding controls as well as comparison of reads mapping to the *UAS-mask*$^{RNAi\text{-}v29541}$ transgene were performed with two-sample two-sided student's t-tests. Gene Ontology analyses was assessed utilizing The Gene Ontology Consortium resources (http://geneontology.org/). Scatterplots and volcano plots (Figure 5) were generated using R-statistical software (CRAN, 2018). For further information on fly lines, software and other key materials, please see Table S1.

RESULTS

Mask is required for morphogenesis of the *Drosophila* retina

The fly eye is a neuroepithelium composed of approximately 750 ommatidia (Cagan and Ready, 1989a; Carthew, 2007; Kumar, 2012; Ready et al., 1976; Wolff and Ready, 1993). Each mature ommatidium contains eight photoreceptor neurons, four cone cells and two primary (1°) pigment cells (Figure 1A). Secondary (2°) and tertiary (3°) pigment cells separate the ommatidia and are precisely positioned to generate an ordered honeycomb-like lattice that spans the eye field (Figure 1A, B). In addition, each eye contains over 600 sensory bristle groups which are embedded within the interommatidial lattice (Figure 1A). An antibody to all Mask isoforms detected the protein throughout the pupal eye in numerous cytoplasmic puncta and at AJs (Figure S1, (Smith et al., 2002)). However, whilst antibody-detection of Mask was abrogated by expression of an RNAi transgene against *mask* (Figure S1C), AJ-localization of Mask, in particular, was not recapitulated in *mask*$^{GFP\text{-}CC00924}$ nor *mask*$^{sfGFP\text{-}TVPTBF}$ retinas (transgenic lines in which the longer Mask isoforms, or all Mask isoforms are potentially GFP-tagged, respectively; Figure S1D, Figure S2A–C; (Sarov et al., 2016)). Yki was similarly observed in numerous apical and cortical puncta in *yki*$^{YFP\text{-}VK37}$ and *yki*$^{sf\text{-}GFP\text{-}TVPTBF}$ retinas and occasionally also at AJs (Figure S2D–E). In addition, a small number of Mask and Yki puncta were observed in the nuclei of cone and pigment cells, and photoreceptors (Figure S2F–Q, and data not shown).

To assess the role of Mask in pupal eye development, we modified its expression using the Gal4/UAS system and *Glass Multimer Reporter-Gal4* (*GMR-Gal4*), which is active in eye tissue after the passage of the morphogenetic furrow that establishes the eye field in the larva (Brand and Perrimon, 1993; Freeman, 1996). Patterning defects in retinas with reduced or increased *mask* expression were then examined and quantified at 40 h APF (ommatidial mis-patterning score (OMS), Figure 1C, Table S3A and B, (Johnson and Cagan, 2009). *UAS-mask*$^{RNAi\text{-}v29541}$, which targets all predicted *mask* transcripts (Figure S1D), generated severe mis-patterning phenotypes including errors in the stereotypical arrangement and size of cone cells, incorrect orientation of ommatidia along the dorsal-ventral axis, unequally-sized 1° cell pairs, and angular rather than curved boundaries between 1°s and neighboring interommatidial cells (Figure 1D). The interommatidial lattice was also disorganized with few correctly-shaped 2° and 3° cells: most were trapezoidal or even triangular, and the

lengths of many lattice-lattice cell boundaries were reduced. Most bristle groups were also mis-positioned and some were located between 1° cell pairs. As discussed in more depth below, we also observed a marked reduction in the density of apical E-cad in all cells of *GMR>mask$^{RNAi\text{-}v29541}$* retinas at 40 h APF (Figure 1D). When expressed together with *UAS-Dcr-2*, a second RNAi transgene, *mask$^{RNAi\text{-}v103411}$*, generated similar albeit more mild patterning defects including modest mis-orientation of ommatidia, straighter 1°-lattice cell boundaries, and mild disruption to the neat organization of the interommatidial cell lattice (Figure 1E, Figure S1D). Ectopic *mask*, induced with *mask^{EY01848}* (Figure S1D) or *UAS-mask^{RA}*, also generated mild patterning defects including disruptions to the formation of correctly-shaped 3°s and grouping of interommatidial lattice cells in two or more rows between ommatidia (Figure 1F–G). In addition, cone cells were occasionally observed in direct contact with lattice cells where 1°s had failed to adhere to each other to fully encircle the cone cell group (Figure 1F', G'). The adults of each of these genotypes displayed "rough eye" phenotypes that corresponded with the degree of pupal eye mis-patterning or OMS scores (Figure 1C, H–L; facet disruption in adult eyes was often more pronounced in the posterior eye where the period of transgene expression had been longest).

UAS-mask$^{RNA\text{-}v29541}$ and *mask^{EY01848}*, which were used for many of our subsequent experiments, effectively modified *mask* transcript expression (Figure S1B–D, Figure S3). In addition, patterning defects in *GMR>mask$^{RNAi\text{-}v29541}$* retinas were significantly enhanced in animals heterozygous for *mask$^{10.22}$* or *mask$^{5.8}$* (Figure S1D, Figure S4), whilst *mask^{EY01848}* reduced *GMR>mask$^{RNAi\text{-}v29541}$* mis-patterning (Figure S4, Table S3C).

Mask promotes survival of retinal cells

Since Hippo signaling has a crucial role in regulating cell survival and mitosis, it was not surprising that the number of interommatidial cells in *GMR>mask$^{RNAi\text{-}v29541}$* retinas at 40 h APF was reduced from an average of 12.21 about an ommatidium in control *GMR>lacZ* retinas to 8.28 (p=1.9×10^{-34}) and ommatidia with one rather than two 1° pigment cells were often found in *GMR>mask$^{RNAi\text{-}v29541}$* retinas (hereafter simply referred to as *GMR>mask^{RNAi}*). These observations were also consistent with the initial description of Mask as a promoter of cell survival (Smith et al., 2002). These defects in cell number did not arise from errors in larval eye development: in *GMR>mask^{RNAi}* larval retinas we observed no change in the final mitotic division of interommatidial cells, which occurs following the passage of the morphogenetic furrow (Figure S5A,B) (Ready et al., 1976; Wolff and Ready, 1991a) and we also observed no increase in apoptosis in *GMR>mask^{RNAi}* larval eye discs (Figure S5C,D). Photoreceptor recruitment was also unperturbed (data not shown). Hence the ommatidial field is correctly established in *GMR>mask^{RNAi}* retinas and the mis-patterning and cell survival defects arise during pupal eye morphogenesis.

A range of signals contribute to the culling of excess interommatidial lattice cells from the eye, a process that begins at ~17–18 h APF and terminates at around 33 h APF. These include apoptosis-inducing signals (Notch, Wingless and Jun N-terminal kinase (JNK) signaling) (Bushnell et al., 2018; Cagan and Ready, 1989b; Cordero et al., 2004; Wolff and Ready, 1991b) and survival-promoting signals (e.g. Epidermal Growth Factor Receptor (EGFR) signaling) (Monserrate and Brachmann, 2007) which integrate to ensure the correct

number of lattice cells remain about each ommatidium. Increased apoptosis was observed in *GMR>mask*^{RNAi} retinas in comparison to control *GMR>lacZ* eyes at 18, 21 and 24 h APF (Figure S6A–C) confirming that Mask promotes lattice cell survival. By 27 h APF, apoptosis in control and *GMR>mask*^{RNAi} retinas was similar (Figure S6A,D,E), suggesting that other survival signals (e.g. EGFR) protect the remaining lattice cells in *GMR>mask*^{RNAi} eyes from apoptosis from this time on. Reducing expression of *yki* similarly reduced lattice cell number (discussed below) and we conclude that Mask and Yki contribute to survival-promoting signals that counterbalance apoptosis to ensure appropriate lattice cell number.

Retinal patterning is independent of changes in lattice cell number

We next questioned whether mis-patterning of *GMR>mask*^{RNAi} retinas was simply a consequence of ectopic apoptosis and, conversely, whether the additional interommatidial cells in *GMR>mask*^{EY01848} retinas disrupted lattice organization. Ectopic cell death was triggered by expression of *reaper* (*rpr*) (White et al., 1994), but as *GMR>rpr* was pupal lethal, we used *Gal4–54C* to express *rpr* only the lattice cells (Bao et al., 2010). At 40 h APF, *54C>rpr* animals had an average of 7.53 lattice cells around an ommatidium (in comparison to 12.17 cells in *54C>lacZ* retinas) yet, as long as at least 5 cells surrounded an ommatidium, the cells adopted contorted shapes to generate a honeycomb lattice and hexagonal ommatidia (Figure 1M,N). Since driving *mask*^{RNAi} transgenes with *Gal4–54C* did not sufficiently reduce *mask* even when co-expressed with *Dcr-2*, we had to compare lattice patterning in *54C>rpr* retinas with that of *GMR>mask*^{RNAi} eyes which had an average of 8.35 interommatidial cells. In this genotype the lattice was markedly distorted and many ommatidia shaped into pentagons (Figure 1O). Many abutting ommatidia not separated by lattice cells were also observed (Figure 1O), a phenotype not observed in *54>rpr* retinas until the number of lattice cells about an ommatidium dropped to below 4 (data not shown). Blocking cell death in *GMR>mask*^{RNAi} retinas via concurrent expression of the cell death inhibitor *Diap1* (Hay et al., 1995) increased lattice cells to an average of 14.85 around an ommatidium, but the lattice was still disorganized with many grouped cells (Figure 1P, green outlines). The ommatidia were seldom neatly hexagonal, often mis-oriented and unequally-sized 1°-cell pairs were frequent (Figure 1P). None of these mis-patterning phenotypes were observed in *GMR>Diap1* retinas (Figure 1R), which had an average of 23.61 lattice cells that nonetheless were organized into single rows around ommatidia and still generated the hexagonal lattice, although the 2° and 3° pigment cell niches were not always correctly patterned. This contrasted with distortions to the lattice in *mask*^{EY01848} retinas (Figure 1S), where the additional interommatidial cells were arranged in groups rather than in single file, and few 3° cells were correctly established. Mis-oriented ommatidia were also observed in *GMR>mask*^{EY01848} retinas (Figure 1S). Taken together, these data indicate that the patterning defects observed when *mask* expression is modified are independent of changes in the number of interommatidial cells. Our data also underscore that lattice patterning is a robust process that adapts to variations in the availability of lattice cells.

Yki and Wts are required for retinal morphogenesis, in concert with Mask

Since Mask interacts with Yki (Kwon et al., 2013; Li et al., 2017; Sansores-Garcia et al., 2013; Sidor et al., 2013), we hypothesized that Mask:Yki complexes contribute to pupal eye

morphogenesis. When co-expressed with *Dcr-2*, *UAS-yki*$^{RNAi\text{-}v104524}$ generated mis-patterning phenotypes that were qualitatively similar to retinas with reduced *mask* expression (Figure 2A–D, Table S3D). Unfortunately *yki*$^{RNAi\text{-}HMS00041}$, a transgene commonly used to reduce *yki* in larval tissues, was pupal-lethal when driven with *GMR-Gal4* and *yki*$^{RNAi\text{-}JF03119}$ generated only very mild eye mis-patterning (not shown). However, in addition to reducing the number of interommatidial cells, *yki*$^{RNAi\text{-}v104524}$ disrupted the lattice, caused misshapen ommatidia that were often not correctly aligned along the dorsal-ventral axis, 1° cell pairs that were unequally sized and mis-positioned bristles. The adult *GMR>yki*$^{RNAi\text{-}v104524}$, *Dcr-2* eyes were accordingly 'rough' and similar to those of *GMR>mask*^{RNAi} adults (Figure 2E–H). Hence Yki, like Mask, is important for the organization of the *Drosophila* retina.

Ectopic *yk*i also generated additional grouped lattice cells and other mild patterning defects similar to those in *GMR>mask* retinas (Figure 2I). In addition, ectopic *yk*i partially suppressed *GMR>mask*^{RNAi} mis-patterning phenotypes (Figure 2J, compare to Figure 2D). However whilst *GMR>mask*^{RNAi} patterning defects were enhanced in *yki* heterozygous retinas (Figure 2L), these effects were mild, as might be expected if little functional Mask, and hence few Mask:Yki complexes, remained in *GMR>mask*^{RNAi} retinas such that further reducing *yki* expression had little effect. These changes in patterning defects were reflected in the disorder of the adult eyes and OMS values (Figure 2H,M–Q, Table S3E). Taken together, our data suggest that Yki and Mask function together to promote eye morphogenesis, although independent roles for Yki are not precluded.

Since Wts is the major negative regulator of Yki, we hypothesized that ectopic *wts* would cause patterning defects similar to those observed when either *mask* or *yki* expression was reduced. Indeed, at 40 h APF, *GMR-wts* retinas were characterized by numerous mis-placed and incorrectly shaped lattice cells, unequal 1°-cell pairs, and mis-oriented ommatidia (Figure 2R). Ectopic *wts* also significantly enhanced *GMR>mask*^{RNAi} mis-patterning at 40 h APF (Figure 2S, Table S3F), whilst a null allele of *wts* significantly reduced *GMR>mask*^{RNAi} defects (Figure 2T,U, Table S3F). As before, these genetic interactions were reflected in the disruptions to the adult eye and OMS values (Figure 2V–Z). In addition, *GMR>mask*^{RNAi} mis-patterning was partially suppressed in tissue heterozygous for mutant alleles for *hippo* (*hpo*), *expanded* (*ex*) or *merlin* (*mer*) (Figure S7, retinas heterozygous for these alleles were correctly patterned). These data support that Hippo pathway activity regulates Mask during pupal eye morphogenesis.

Mask regulates AJ distribution and cytoskeletal structures in the retina

To better understand the cause of mis-patterning in retinas with reduced *mask* expression, we considered the requirement for Mask for correct AJ distribution and density. Loss of function *mask* clones failed to survive and *mask*$^{RNAi\text{-}v29541}$ clones (generated using the standard weaker *actin-Gal4* driver) had little phenotype. However the dorsal specific *mirror-Gal4* driver (Figure S8A,B) (McNeill et al., 1997) generated a gradient of *mask*$^{RNAi\text{-}v33396}$ or *mask*$^{RNAi\text{-}v29541}$ expression that mildly disrupted distribution of AJs, assessed at 24 h APF (Figure S8C–H, patterning was also mildly disrupted). Specifically, AJs were not evenly distributed about the entire periphery of 1°s and lattice cells, leaving numerous 'gaps'

in E-cad distribution (Figure S8E,H). Since transgenes were only weakly expressed in *mirr>mask*^{RNAi} pupae and these rarely survived beyond 24 h APF, we utilized *GMR-Gal4* for all further analyses, although this restricted our comparisons to between retinas.

In wild type (or control) eyes, early patterning is characterized by local cell rearrangements and changes in cell shape and size, and coincident with this, AJs are not uniformly distributed (Figure 3A–D) (Johnson, 2020). This likely reflects AJ remodeling or the formation of nascent junctions that have not yet been stabilized (Guillot and Lecuit, 2013). Reducing *mask* significantly increased the frequency and persistence of gaps in E-cad/AJ distribution, although this became less obvious at junctions between 1° cell pairs from 27 h APF (Figure 3E–J). In addition, significantly less E-cad was detected at AJs in *GMR>mask*$^{RNAi\text{-}v29541}$ retinas at 24 and 40 h APF (Figure 1D, 3K). We conclude that Mask is critical for establishing, securing or maintaining AJs.

Similar defects in AJ organization were observed in *GMR>yki*$^{RNAi\text{-}v104524}$, *Dcr-2* and *GMR-wts* retinas (Figure 4A–D). In addition, whilst *yki* alleles failed to modify *mask*^{RNAi} induced AJ disruption, ectopic *yki* significantly rescued these defects (Figure 4E–J,O). A *wts* null allele similarly rescued AJ organization in *GMR>mask*^{RNAi} retinas and AJ defects were severely augmented by ectopic *wts* (Figure 4K–N,P). These data suggest that Hippo pathway activity must be correctly controlled for the appropriate regulation of adhesion during eye morphogenesis.

Accordingly, adhesion defects generated when *mask*, *yki* or *wts* expression were modified could account for retinal disorder since compromising AJ dynamics or stability would impair morphogenetic processes necessary to position and shape retinal cells (Figures 1, 2). Indeed, directly targeting AJs by reducing *E-cad* expression disrupted eye patterning (Figure S9), but phenotypic similarities between *GMR>E-cad*^{RNAi}, *GMR>mask*^{RNAi}, *GMR>yki*^{RNAi} and *GMR-wts* retinas were limited. Specifically, reducing *E-cad* led to lattice cells that were poorly organized, but in *GMR>E-cad*^{RNAi} retinas, 1° cell pairs were generally equal in size and most boundaries between 1° and lattice cells were curved rather than straight, as frequently observed in *GMR>mask*^{RNAi} retinas. These data argue that morphogenetic defects in retinas with less Mask or Yki activity do not originate only from changes in AJ organization.

Given the functional importance of interactions between AJs and the cytoskeleton, we next examined actin and myosin structures in *GMR>mask*^{RNAi} retinas. At both 24 and 40 h APF, the density of F-actin greatly increased (Figure S10A–E), and the accumulation of non-muscle myosin II (NMII) decreased (Figure S10F–J) when *mask* expression was reduced. In control 1° cells, the apical actin cytoskeleton is strikingly organized into numerous F-actin structures that appear to tile across the cells' width at right angles to the 1° cell-lattice cell interface by 40 h APF (Figure S10C). The functional importance of these F-actin structures has not been explored but we note that in *GMR>mask*^{RNAi} retinas they were entirely disrupted and 1° cells were seldom correctly sized or shaped, suggesting a role in determining or maintaining cell architecture (Figure S10D). In control 1°s, NMII accumulated along the 'concave' surfaces at 1°-lattice cell interfaces at 40 h APF (Figure S10H), correlating with a model where myosin-mediated contractility contributes to the

rounded shape of 1°s. Accordingly, in *GMR>mask*^{RNAi} retinas approximately equal accumulation of NMII in abutting 1°-lattice cell neighbors could account for the straighter form of these cell interfaces (Figure S10I). NMII puncta also accumulated through the cytoplasm of control lattice cells at 40 h APF (Figure S10H), but not in *GMR>mask*^{RNAi} lattice cells (Figure S10I), which were also marked by a striking increase in F-actin (Figure S10D). We predict that these disruptions to the cytoskeleton contribute to the irregular cell shapes in *GMR>mask*^{RNAi} retinas and propose that Mask is an important regulator of the cytoskeleton in the eye.

Mask regulates genes associated with adhesion and the cytoskeleton

To identify genes regulated by Mask that contribute to retinal morphogenesis, we used RNA-sequencing to assess genome-wide gene expression at 24 h APF in *GMR>GFP*^{RNAi}, *GMR>mask*^{RNAi}, *GMR>GFP* and *GMR>mask* retinas (Figure S11). This generated 5.22×10^8 sequence reads, with a range of 35,255,405 to 48,935,181 mapped reads per sample (with 92.12 to 93.29% reads mapping to the genome), suggesting that we had appropriate read-depth for confident quantification of most of the expressed genome (Table S5). Reducing *mask* resulted in significant changes in the expression of 1674 genes (Table S6, Figure 5A,B), and in tissue with ectopic *mask*, 255 genes were significantly differentially expressed (Table S7, Figure 5A,B). Expression of 129 loci was significantly modified in response to both reduced and increased *mask*. In addition, the expression of twelve known targets of Yki or Hippo pathway activity changed in *GMR>mask*^{RNAi}, although these changes were not all statistically significant (Table S8).

Gene Ontology (GO) analyses revealed that Mask regulates genes involved in a variety of biological processes (Table S9) including genes associated with adhesion or with roles in the actin cytoskeleton (Tables S6 and S9), although expression of core AJ components (*shotgun*, which encodes *Drosophila* E-cad, and the Catenin proteins) was not significantly changed. Further, ectopic *E-cad* failed to rescue *GMR>mask*^{RNAi} mis-patterning, which was also not modified in retinas heterozygous for *E-cad* (*shg)* (Figure S12,Table S3G). Hence, we conclude that rather than regulating transcription of core AJ proteins, Mask instead contributes to mechanisms that influence AJ assembly or stability. Amongst the loci that could mediate this were *FER tyrosine kinase* (*FER*) and *Vinculin* (*Vinc*) which were repressed and promoted in the presence of Mask, respectively (Tables S6, S10). FER has been implicated in the phosphorylation and degradation of β-catenin (Murray et al., 2006; Piedra et al., 2003; Rosato et al., 1998) and Vinc contributes to AJ formation and is recruited to AJs in response to mechanical stress (Galbraith et al., 2002; Le Duc et al., 2010; Leerberg et al., 2014; Opazo Saez et al., 2004; Taguchi et al., 2011). We discuss our initial investigations into the roles of these loci during retinal morphogenesis in more detail below.

Amongst the transcriptional changes detected in *GMR>mask*^{RNAi} retinas that could account for disruptions to F-actin structures were *Abelson interacting protein* (*Abi*) ($\log_2$ fold change in expression = 0.42), which regulates actin dynamics through the WASP and WAVE complexes (Bogdan et al., 2005); *washout* (*wash*) ($\log_2$ fold change = 0.63), which crosslinks F-actin and microtubules and is required for maintaining the actin cytoskeleton in the ovary (Liu et al., 2009); and RhoGEF3 ($\log_2$ fold change = −0.40) and RhoGEF4 ($\log_2$

fold change = 0.56), which have been implicated in activating Rac1 (Nakamura et al., 2017) and RhoA (Nahm et al., 2006). Changes in expression of *Shroom* ($\log_2$ fold change = −0.41), which acts through Rho-kinase to promote NMII activity (Nishimura and Takeichi, 2008), may account for the reduced accumulation of NMII in *GMR>mask*^{RNAi} retinas (Figure S10G,I).

qRT-PCR confirmed that *Vinc, FER*, *Abi* and *wash* expression was similarly regulated by Yki and Mask in pupal retinas (Figure 5C), suggesting that these loci are regulated by Mask:Yki complexes, although this regulation may be indirect. However, whilst Mask promoted *Shroom* expression, it was antagonized by Yki (Figure 5C), suggesting independent roles for Mask and Yki in *Shroom* regulation.

Repression of *FER* downstream of Mask is essential for eye morphogenesis

FER expression significantly increased in *GMR>mask*^{RNAi} retinas ($\log_2$ fold change = 0.34, Table S6) and decreased, although not significantly, in *GMR>mask* retinas ($\log_2$ fold change= −0.19, Table S7). Because FER has been implicated in β-catenin phosphorylation and consequent degradation (Murray et al., 2006; Piedra et al., 2003; Rosato et al., 1998), we hypothesized that elevated *FER* would contribute to AJ disruption when *mask* was reduced. Accordingly ectopic expression of *FER* generated discontinuous distribution of E-cad in retinal cells at 24 h APF similar to those observed in *GMR>mask*^{RNAi} tissue (Figure 6A–B). Ectopic *FER* also amplified errors in AJ distribution in *GMR>mask*^{RNAi} retinas (Figure 6C–E), increased the number of patterning errors observed by 40 h APF (Figure 6F–J, Table 3H), and enhanced the consequent roughness of the adult eye (Figure 6K–N, Table 3H). In addition, *GMR>FER* retinas were characterized by mild disorganization of the lattice and patterning errors commonly observed in retinas with reduced *mask* (Figure 6G), although additional lattice cells were also common, possibly due to ectopic Wg signaling consequent to reduced β-catenin (Chen et al., 2014). In the pupal retina, Wg activity contributes to apoptosis of excess lattice cells (Cordero et al., 2004; Lin et al., 2004) and, accordingly, reducing *FER* expression led to the occasional missing lattice cell and also generated mild patterning defects that qualitatively resembled phenotypes observed in *GMR>mask* retinas (Figure S13, Table S3I). Further, disruptions to AJs in *GMR>mask*^{RNAi} retinas were mainly suppressed in tissue also heterozygous for *FER*^{X21} (Figure 6E,O–P) and mis-patterning was significantly suppressed and the adult eye relatively undisrupted (Figure 6Q–T, Table S3H). Taken together, our data indicate that suppression of *FER* downstream of Mask activity is essential for correct AJ distribution and eye morphogenesis and ectopic *FER* contributes to patterning defects in *GMR>mask*^{RNAi} retinas.

Vinculin is an effector of Mask during eye patterning

Expression of *Vinc* was significantly reduced in *GMR>mask*^{RNAi} retinas ($\log_2$ fold change = −0.73, Table S6). Given the role of Vinc in fortifying AJs (Huveneers et al., 2012; Taguchi et al., 2011; Yonemura et al., 2010), we then tested the hypothesis that *Vinc* was amongst the genes promoted by Mask that favored AJ stabilization during eye morphogenesis. Indeed, ectopic *Vinc* partially rescued defects in AJ distribution in *GMR>mask*^{RNAi} retinas at 24 h APF (Figure 7A–E) and this correlated with significantly fewer patterning defects at 40 h APF (Figure 7F–J, Table S3J) and improved organization of the adult eye (Figure 7K–N).

Conversely, in *GMR>mask*^{RNAi} retinas also heterozygous for *Vinc*, gaps in AJs were wider and more frequent at 24 h APF (Figure 7E,O–P), and mis-patterning defects were modestly enhanced at 40 h APF and in adults (Figure 7J, Q–T, Table S3J). Patterning analyses (Table S3J) also suggested a greater requirement for Mask-Vinc function in 1° cells than in lattice or bristle cell groups. Specifically, in *GMR>mask*^{RNAi} retinas, errors in the number of 1°s (two per ommatidium) occurred with a frequency of 0.16 (SD=0.37), and ectopic *Vinc* reduced this to 0.04 (SD=0.20) whilst in *Vinc* heterozygotes this frequency increased to 0.23 (SD=0.43). Further, in *GMR>mask*^{RNAi} retinas the junctions between 1° pairs were compromised at a frequency of 0.04 (SD=0.20) and 1° pairs remained 'open', leaving cone cells in contact with neighboring lattice or bristle cells, at a frequency of 0.04 (SD=0.20). These phenotypes were not modified by ectopic *Vinc* but in *Vinc* heterozygotes the frequency of shorter or disrupted 1°:1° junctions increased to 0.19 (SD=0.40) and 'open' 1° pairs were present at a frequency of 0.27 (SD=0.61). Taken together, our data allude to an important role for Vinculin in the formation of stable junctions, especially between neighboring 1°s, during eye patterning.

Mask regulates a set of genes that promote cell survival

Expression of the Yki target *Diap1* is commonly used to assess Hippo pathway activity and considered central to Yki's role in limiting apoptosis (Huang et al., 2005). However, our transcriptome analyses detected only modest reduction in *Diap1* expression ($\log_2$ Fold change = −0.05) in *GMR>mask*^{RNAi} retinas (Table S6, S8). This observation is consistent with a previous study where *Diap1* expression was not reduced in larval eye discs despite increased Hpo, Sav or Wts activity (Verghese et al., 2012). Instead we identified changes in expression of a large number of other genes associated with apoptosis or cell survival in *GMR>mask*^{RNAi} retinas (Table S11). These included significant increases in the expression of core components of the apoptosis machinery, including *grim, rpr* and *Death regulator Nedd2-like caspase* (*Dronc*, which conversely has previously been shown to decrease when Yki was activated (Verghese et al., 2012)). In addition, we detected gene expression changes that would modify signaling pathways associated with apoptosis or survival of lattice cells in the pupal eye. These changes included increased expression of *wingless* and its receptor *frizzled* and modified expression of multiple components of the Notch signaling pathway (Table S11). Both Notch and Wingless signaling promote apoptosis of lattice cells (Cagan and Ready, 1989b; Cordero et al., 2004; Lin et al., 2004; Miller and Cagan, 1998). Further, expression of *Egfr*, which promotes retinal cell survival (Domínguez et al., 1998; Freeman, 1996; Miller and Cagan, 1998), was decreased (Table S11). Hence, a comprehensive set of cell-death and survival factors are regulated downstream of Mask during pupal eye morphogenesis, underscoring a broad role for Mask in promoting cell survival.

Diverse signal transduction pathways are modified by Mask

Our RNA-sequencing data revealed that an array of signaling pathway components are modified by Mask activity in the retina (Table S12), although many of these changes may be indirect or reflect interactions between signaling networks. Nonetheless, it is striking that expression of multiple components of the Hedgehog, Notch, RTK, TGFβ, Toll and Wnt signaling pathways were modified in *GMR>mask*^{RNAi} retinas, as well as numerous GPCRs (Table S12). It is plausible that the transcriptional changes in the EGF-Receptor, and other

RTK components, identified in our analyses account for the initial description of Mask as a modifier of RTK signaling (Smith et al., 2002). Given the importance of RTK signaling in the *Drosophila* pupal eye (Malartre, 2016), these transcriptional changes would contribute, no doubt, to the complexity of the patterning defects observed when *mask* was reduced during eye morphogenesis. We also observed changes in the expression of several components of the planar cell polarity (PCP) system (*diego* (*dgo*), *Van Gogh* (*Vang*), *frizzled* (*fz*) and *fat* (*ft*)), which could account for the disrupted orientation of many ommatidia in *GMR>mask*^{RNAi} retinas.

In addition to its role in PCP, Fat also functions to modify Hippo signaling, as does *crumbs*, which was also expressed at lower levels in *GMR>mask*^{RNAi} retinas (Table S12). The expression of two transcription factors that complex with Yki, *Mothers against dpp* (*Mad*) and *scalloped* (*sd*), was also modified in *GMR>mask*^{RNAi} tissue ($\log_2$ fold change= 0.37, (Table S6 and S12); and −0.29, (Table S6)). Hence, multiple feedback loops appear to be triggered by Mask in the retina to transcriptionally modulate Hippo pathway activity.

Further studies are required to clarify whether the signaling pathways and networks modified by Mask function in specific retinal cell types or throughout the eye. For example, we note that several Semaphorins as well as *roundabout 1* (*robo1*) were modified by Mask (Table S12). Given the role of these gene families in axon guidance, it is plausible that these function in the organization of axons projected by photoreceptor or bristle neurons (Hu and Zhu, 2018; Seiradake et al., 2016).

DISCUSSION

Drosophila epithelia have been used extensively to characterize the role of Hippo signaling in tissue growth (Irvine and Harvey, 2015; Snigdha et al., 2019), but here we describe Hippo as a major contributor to epithelial morphogenesis. In assessing the contribution of Yki and its cofactor Mask to tissue morphogenesis and cell architecture, we used an approach that modified their activity mainly after the eye field and photoreceptors were established and mitosis had ceased. Hence, we avoided modifying Hippo pathway activity early in eye development, which profoundly alters cell proliferation and also severely modifies activity of the retinal determination gene network to perturb early eye patterning, photoreceptor selection, and eye size (Wittkorn et al., 2015).

Using RNA-seq, we identified many genes that require Mask activity for their correct expression, although these expression changes were captured in whole retinas at 24 h APF and additional investigations are required to determine which expression changes are cell-specific (pigment cells, photoreceptors, neurons and support cells of the bristle groups; Table S6 and S9). We modified *mask* for our transcriptional analyses rather than *yki* because, in our hands, the available RNAi transgenes that target *mask* were more effective. Indeed, we detected both Mask and Yki in most retinal cell nuclei (although sparsely, Figure S2) and Mask has previously been shown to promote transcription of Yki target genes, possibly via regulating nuclear localization of Yki (Sansores-Garcia et al., 2013; Sidor et al., 2019; Sidor et al., 2013). Accordingly, several loci already identified as Yki/YAP/TAZ targets were also modified by Mask (Table S8). That some of these Yki targets were not significantly

modified in our experimental set-up may reflect differences in the transcriptional potential of post-mitotic versus mitotic tissues. Further, our qRT-PCR analyses confirmed that several loci we identified - *FER*, *Vinc*, *Abi* and *wash* - were similarly modified by Mask and Yki (Figure 5C). Hence we predict that many transcriptional changes we identified downstream of Mask (Tables S6 and S7) were consequent to modified Yki activity. Of course some are likely to be Yki-independent. For example, we found that *Shroom* expression, which required Mask, was instead potentially suppressed by Yki (Figure 5C). We also note that Mask has been identified as a modifier of splicing (Brooks et al., 2015) and expect that loss of this function contributed complexity to the transcriptional changes and patterning defects in *GMR>mask*^{RNAi} retinas.

In particular, our *in vivo* data emphasize that Mask, Yki and Wts promote AJ assembly or stability in retinal cells (Figure 3, 4). We also found that Mask is essential for the organization of actin and NMII at both 24 and 40 h APF (Figure S10). Specifically, Mask antagonizes F-actin and promotes NMII accumulation. These data are consistent with the work of Kim and colleagues, who found that YAP is required during angiogenesis in the murine retina and brain for maintaining VE-cadherin levels and distribution and actin/myosin organization (Kim et al., 2017a). In contrast, several studies have shown that YAP or Mask1 antagonize cell adhesion and promote cell migration (Bai et al., 2016; Calvo et al., 2013; Dhyani et al., 2015; Yao et al., 2018; Zhou et al., 2019), but it is plausible that these inconsistencies reflect tissue or context-specific outcomes for Mask/Mask1 and Yki/YAP activities.

Of the many adhesion-related genes modified by Mask activity (Table S6, 10), we chose to focus on two for immediate validation. We found that Mask activity reduced *FER* expression, and since FER phosphorylates β-Catenin to promote its degradation (Murray et al., 2006; Piedra et al., 2003; Rosato et al., 1998), we predict that the excess FER present in *GMR>mask*^{RNAi} retinas leads to rapid turnover of AJs, contributing to reduced AJ density and errors in AJ distribution (Figure 6). In contrast, Mask promoted *Vinc* expression. Since Vinc has an established role in fortifying connections between the Catenins and the actin cytoskeleton when AJs are subject to mechanical stress (Bershadsky et al., 2003; Galbraith et al., 2002; Huveneers et al., 2012; Opazo Saez et al., 2004; Taguchi et al., 2011; Yonemura et al., 2010), we expect that reduced *Vinc* expression in *GMR>mask*^{RNAi} retinas compromised this response (Figure 7). However, these hypotheses require validation.

Diverse studies have established that changes in adhesion and the actin-myosin cytoskeleton, can profoundly modify YAP/Yki activity (Aragona et al., 2013; Calvo et al., 2013; Dupont et al., 2011; Fernández et al., 2011; Gaspar et al., 2015; Kim et al., 2011; Matsui and Lai, 2013; Rauskolb et al., 2014; Sansores-Garcia et al., 2011; Schlegelmilch et al., 2011; Silvis et al., 2011; Zhao et al., 2012). However, our examination of Mask and Yki in the pupal eye, as well studies that examined YAP's role in cell invasion/migration and adhesion, identified many genes associated with actin, myosin and adhesion as transcriptional targets of Hippo activity (Bai et al., 2016; Calvo et al., 2013; Kim et al., 2017a; Lin et al., 2017; Yao et al., 2018). Hence, Hippo signaling appears to utilize a feedback mechanism to coordinate transcriptional and cytoskeletal/junction activities. Indeed, the expression of numerous Hippo pathway proteins was also modified in *GMR>mask*^{RNAi} retinas, including *crb*, *ft* and

sd (expression of these three loci was significantly decreased) and *mad* (expression significantly increased), hinting at multiple opportunities for feedback regulation of Hippo signaling by Mask. Crumbs has previously been identified as a transcriptional target of Yki (Genevet et al., 2009; Zhu et al., 2015b).

Not all feedback between Hippo pathway activity and the cytoskeleton or adhesion is mediated through changes in gene expression. Indeed, Wts directly impacts actin polarization in border cells of the fly ovary via phosphorylation of Enabled, to promote border cell migration (Lucas et al., 2013). In addition, cytoplasmic Yki has been shown to interact with Strn-Mlck to promote NMII accumulation and activation at the apical cortex of cells in the *Drosophila* larval wing disc, contributing to the generation of tensile forces in this tissue (Xu et al., 2018). It is therefore very plausible that the dense apical pool of Mask and Yki we identified in *Drosophila* retinas (Figure S1 and S2) similarly contributes to apical myosin-structures and hence cortical tension in this tissue. Indeed, the disruption of NMII accumulation that we observed in $GMR{>}mask^{RNAi}$ retinas could reflect this role (Figure S10F–I). Although not recapitulated in $mask^{GFP}$ fly lines, we also detected Mask at AJs using a Mask antibody (Figure S1). Similarly, we observed a subset of Yki at AJs (Figure S2), consistent with the maintenance of inactive YAP at AJs via interactions with 14-3-3 and α-catenin (Schlegelmilch et al., 2011). It is plausible then that a subset of Mask is maintained in complexes with Yki at AJs, but this hypothesis, as well as the role of Mask at this location, remains to be tested.

Our RNA sequencing analyses also identified a large number of genes that regulate cell death that are modified downstream of Mask activity (Table S11). These included core components of the apoptosis machinery (Denton and Kumar, 2015) including *Dronc*, *grim*, *Dark* and *rpr*, which were expressed at higher levels in $GMR{>}mask^{RNAi}$ retinas. Expression of *Diap1*, which is an established target of Yki (Huang et al., 2005) was modestly reduced in these retinas (Table S8). We also found changes in transcription that would enhance signaling pathways that promote apoptosis in the fly eye (eg. Wg signaling) (Cordero et al., 2004) and impede those that protect cells from death (eg. EGFR signaling) (Miller and Cagan, 1998; Monserrate and Brachmann, 2007). Taken together, these transcriptional changes demonstrate and account for the powerful impact of Hippo pathway activity in regulating cell survival.

Inevitably, many of the genes identified in our RNA-sequencing analyses may not be direct targets of Mask or Mask:Yki transcriptional complexes but instead targets of the signaling pathways modified by Mask (including Hedgehog, Notch, RTK, TGFβ, Toll, and Wnt signaling pathways; Table S12). Indeed, Hippo signaling has also been shown in other systems to facilitate transcription of components of the Notch, EGFR, and JAK-STAT pathways (Ren et al., 2010a; Yu et al., 2008) and, perhaps not surprisingly, significant crosstalk between Hippo and other signaling pathways has been described (Kim et al., 2017b; Polesello and Tapon, 2007; Reddy and Irvine, 2013). These signaling networks surely add further complexity to the role of Hippo signaling in tissue morphogenesis.

Supplementary Material

Refer to Web version on PubMed Central for supplementary material.

ACKNOWLEGEMENTS

We thank our reviewers for helpful comments on our work, and the BDSC (NIH P400D018537), the VDRC (Dietzl et al., 2007), Iswar Hariharan, Mike Simon, Ken Irvine, Ulrich Tepass, Chunlai Wu, Richard Fehon, Cathie Pfleger and Nick Brown for fly lines or antibodies. We also thank Arielle Ashley, Redwan Bhuiyan and Kayla Jaikaran for technical assistance, and Cathie Pfleger, Michael Weir and members of the Johnson and Coolon Labs for helpful discussion. Lucas Coolon provided artistic assistance in matching colors in Figure 5. This work was supported by R15GM114729.

REFERENCES

Afgan E, Baker D, Batut B, van den Beek M, Bouvier D, Cech M, Chilton J, Clements D, Coraor N, Grüning BA, et al. (2018). The Galaxy platform for accessible, reproducible and collaborative biomedical analyses: 2018 update. Nucleic acids research 46, W537–W544. [PubMed: 29790989]

Andrews S (2010). FastQC: a quality control tool for high throughput sequence data.

Aragona M, Panciera T, Manfrin A, Giulitti S, Michielin F, Elvassore N, Dupont S, and Piccolo S (2013). A mechanical checkpoint controls multicellular growth through YAP/TAZ regulation by actin-processing factors. Cell 154, 1047–1059. [PubMed: 23954413]

Bai H, Zhu Q, Surcel A, Luo T, Ren Y, Guan B, Liu Y, Wu N, Joseph NE, and Wang T-L (2016). Yes-Associated Protein impacts adherens junction assembly through regulating actin cytoskeleton organization. American Journal of Physiology-Gastrointestinal and Liver Physiology, ajpgi. 00027.02016.

Bao S, Fischbach K-F, Corbin V, and Cagan RL (2010). Preferential adhesion maintains separation of ommatidia in the Drosophila eye. Developmental Biology 344, 948–956. [PubMed: 20599904]

Bershadsky AD, Balaban NQ, and Geiger B (2003). Adhesion-dependent cell mechanosensitivity. Annual review of cell and developmental biology 19, 677–695.

Bogdan S, Stephan R, Löbke C, Mertens A, and Klämbt C (2005). Abi activates WASP to promote sensory organ development. Nature cell biology 7, 977–984. [PubMed: 16155589]

Boopathy GT, and Hong W (2019). Role of hippo pathway-Yap/Taz signaling in angiogenesis. Front Cell Dev Biol 7.

Brand AH, and Perrimon N (1993). Targeted gene expression as a means of altering cell fates and generating dominant phenotypes. Development 118, 401–415. [PubMed: 8223268]

Brooks AN, Duff MO, May G, Yang L, Bolisetty M, Landolin J, Wan K, Sandler J, Booth BW, Celniker SE, et al. (2015). Regulation of alternative splicing in Drosophila by 56 RNA binding proteins. Genome research 25, 1771–1780. [PubMed: 26294686]

Bushnell HL, Feiler CE, Ketosugbo KF, Hellerman MB, Nazzaro VL, and Johnson RI (2018). JNK is antagonized to ensure the correct number of interommatidial cells pattern the Drosophila retina. Developmental Biology 433, 94–107. [PubMed: 29133184]

Cagan RL, and Ready DF (1989a). The emergence of order in the Drosophila pupal retina. Developmental biology 136, 346–362. [PubMed: 2511048]

Cagan RL, and Ready DF (1989b). Notch is required for successive cell decisions in the developing Drosophila retina. Genes & development 3, 1099–1112. [PubMed: 2792755]

Calvo F, Ege N, Grande-Garcia A, Hooper S, Jenkins RP, Chaudhry SI, Harrington K, Williamson P, Moeendarbary E, and Charras G (2013). Mechanotransduction and YAP-dependent matrix remodelling is required for the generation and maintenance of cancer-associated fibroblasts. Nature cell biology 15, 637. [PubMed: 23708000]

Carthew RW (2007). Pattern formation in the Drosophila eye. Current opinion in genetics & development 17, 309–313. [PubMed: 17618111]

Chen Q, Su Y, Wesslowski J, Hagemann AI, Ramialison M, Wittbrodt J, Scholpp S, and Davidson G (2014). Tyrosine phosphorylation of LRP6 by Src and Fer inhibits Wnt/β-catenin signalling. EMBO reports 15, 1254–1267. [PubMed: 25391905]

Cordero J, Jassim O, Bao S, and Cagan R (2004). A role for wingless in an early pupal cell death event that contributes to patterning the Drosophila eye. Mechanisms of development 121, 1523–1530. [PubMed: 15511643]

CRAN (2018). R: A language and environment for statistical computing (Vienna, Austria: R Foundation for Statistical Computing).

DeAngelis MW, and Johnson RI (2019). Dissection of the Drosophila Pupal Retina for Immunohistochemistry, Western Analysis, and RNA Isolation. JoVE (Journal of Visualized Experiments), e59299.

Deng H, Wang W, Yu J, Zheng Y, Qing Y, and Pan D (2015). Spectrin regulates Hippo signaling by modulating cortical actomyosin activity. Elife 4, e06567. [PubMed: 25826608]

Denton D, and Kumar S (2015). Studying apoptosis in Drosophila. Cold Spring Harbor Protocols 2015, pdb. top070433.

Dhyani A, Machado-Neto JA, Favaro P, and Saad STO (2015). ANKHD1 represses p21 (WAF1/CIP1) promoter and promotes multiple myeloma cell growth. European journal of cancer 51, 252–259. [PubMed: 25483783]

Dietzl G, Chen D, Schnorrer F, Su K-C, Barinova Y, Fellner M, Gasser B, Kinsey K, Oppel S, Scheiblauer S, et al. (2007). A genome-wide transgenic RNAi library for conditional gene inactivation in Drosophila. Nature 448, 151–156. [PubMed: 17625558]

Domínguez M, Wasserman JD, and Freeman M (1998). Multiple functions of the EGF receptor in Drosophila eye development. Current biology 8, 1039–1048. [PubMed: 9768358]

Dong J, Feldmann G, Huang J, Wu S, Zhang N, Comerford SA, Gayyed MF, Anders RA, Maitra A, and Pan D (2007). Elucidation of a universal size-control mechanism in Drosophila and mammals. Cell 130, 1120–1133. [PubMed: 17889654]

Dupont S, Morsut L, Aragona M, Enzo E, Giulitti S, Cordenonsi M, Zanconato F, Le Digabel J, Forcato M, and Bicciato S (2011). Role of YAP/TAZ in mechanotransduction. Nature 474, 179–183. [PubMed: 21654799]

Fernández BG, Gaspar P, Brás-Pereira C, Jezowska B, Rebelo SR, and Janody F (2011). Actin-Capping Protein and the Hippo pathway regulate F-actin and tissue growth in Drosophila. Development 138, 2337–2346. [PubMed: 21525075]

Fletcher GC, Elbediwy A, Khanal I, Ribeiro PS, Tapon N, and Thompson BJ (2015). The Spectrin cytoskeleton regulates the Hippo signalling pathway. The EMBO journal 34, 940–954. [PubMed: 25712476]

Freeman M (1996). Reiterative use of the EGF receptor triggers differentiation of all cell types in the Drosophila eye. Cell 87, 651–660. [PubMed: 8929534]

Galbraith CG, Yamada KM, and Sheetz MP (2002). The relationship between force and focal complex development. J Cell Biol 159, 695–705. [PubMed: 12446745]

Gaspar P, Holder MV, Aerne BL, Janody F, and Tapon N (2015). Zyxin antagonizes the FERM protein expanded to couple F-actin and Yorkie-dependent organ growth. Current biology 25, 679–689. [PubMed: 25728696]

Genevet A, Polesello C, Blight K, Robertson F, Collinson LM, Pichaud F, and Tapon N (2009). The Hippo pathway regulates apical-domain size independently of its growth-control function. J Cell Sci 122, 2360–2370. [PubMed: 19531586]

Godt D, and Tepass U (1998). Drosophila oocyte localization is mediated by differential cadherin-based adhesion. Nature 395, 387. [PubMed: 9759729]

Goulev Y, Fauny JD, Gonzalez-Marti B, Flagiello D, Silber J, and Zider A (2008). SCALLOPED interacts with YORKIE, the nuclear effector of the hippo tumor-suppressor pathway in Drosophila. Current Biology 18, 435–441. [PubMed: 18313299]

Guillot C, and Lecuit T (2013). Mechanics of epithelial tissue homeostasis and morphogenesis. Science 340, 1185–1189. [PubMed: 23744939]

Harvey KF, Pfleger CM, and Hariharan IK (2003). The Drosophila Mst ortholog, hippo, restricts growth and cell proliferation and promotes apoptosis. Cell 114, 457–467. [PubMed: 12941274]

Hay BA, Wassarman DA, and Rubin GM (1995). Drosophila homologs of baculovirus inhibitor of apoptosis proteins function to block cell death. Cell 83, 1253–1262. [PubMed: 8548811]

Hu S, and Zhu L (2018). Semaphorins and Their Receptors: From Axonal Guidance to Atherosclerosis. Frontiers in Physiology 9.

Huang J, Wu S, Barrera J, Matthews K, and Pan D (2005). The Hippo signaling pathway coordinately regulates cell proliferation and apoptosis by inactivating Yorkie, the Drosophila Homolog of YAP. Cell 122, 421–434. [PubMed: 16096061]

Huveneers S, Oldenburg J, Spanjaard E, van der Krogt G, Grigoriev I, Akhmanova A, Rehmann H, and de Rooij J (2012). Vinculin associates with endothelial VE-cadherin junctions to control force-dependent remodeling. J Cell Biol 196, 641–652. [PubMed: 22391038]

Irvine KD, and Harvey KF (2015). Control of organ growth by patterning and hippo signaling in Drosophila. Cold Spring Harbor perspectives in biology 7, a019224. [PubMed: 26032720]

Johnson RI (2020). Molecular Genetics of Axial Patterning, Growth and Disease in Drosophila eye (Springer).

Johnson RI, and Cagan RL (2009). A Quantitative Method to Analyze Drosophila Pupal Eye Patterning. PLoS ONE 4, e7008. [PubMed: 19753121]

Johnson RI, Sedgwick A, D'Souza-Schorey C, and Cagan RL (2011). Role for a Cindr–Arf6 axis in patterning emerging epithelia. Molecular biology of the cell 22, 4513–4526. [PubMed: 21976699]

Kim J, Kim YH, Kim J, Bae H, Lee D-H, Kim KH, Hong SP, Jang SP, Kubota Y, and Kwon Y-G (2017a). YAP/TAZ regulates sprouting angiogenesis and vascular barrier maturation. The Journal of clinical investigation 127, 3441–3461. [PubMed: 28805663]

Kim N-G, Koh E, Chen X, and Gumbiner BM (2011). E-cadherin mediates contact inhibition of proliferation through Hippo signaling-pathway components. Proceedings of the National Academy of Sciences 108, 11930–11935.

Kim W, Khan SK, Gvozdenovic-Jeremic J, Kim Y, Dahlman J, Kim H, Park O, Ishitani T, Jho E. h., and Gao B (2017b). Hippo signaling interactions with Wnt/β-catenin and Notch signaling repress liver tumorigenesis. The Journal of clinical investigation 127, 137–152. [PubMed: 27869648]

Klapholz B, Herbert SL, Wellmann J, Johnson R, Parsons M, and Brown NH (2015). Alternative mechanisms for talin to mediate integrin function. Current biology 25, 847–857. [PubMed: 25754646]

Kumar JP (2012). Building an ommatidium one cell at a time. Developmental Dynamics 241, 136–149. [PubMed: 22174084]

Kwon Y, Vinayagam A, Sun X, Dephoure N, Gygi SP, Hong P, and Perrimon N (2013). The Hippo signaling pathway interactome. Science 342, 737–740. [PubMed: 24114784]

Langmead B, and Salzberg SL (2012). Fast gapped-read alignment with Bowtie 2. Nature methods 9, 357. [PubMed: 22388286]

Lanno SM, Gregory SM, Shimshak SJ, Alverson MK, Chiu K, Feil AL, Findley MG, Forman TE, Gordon JT, and Ho J (2017). Transcriptomic Analysis of Octanoic Acid Response in Drosophila sechellia Using RNA-Sequencing. G3: Genes, Genomes, Genetics 7, 3867–3873.

Le Duc Q, Shi Q, Blonk I, Sonnenberg A, Wang N, Leckband D, and De Rooij J (2010). Vinculin potentiates E-cadherin mechanosensing and is recruited to actin-anchored sites within adherens junctions in a myosin II–dependent manner. The Journal of cell biology 189, 1107–1115. [PubMed: 20584916]

Leerberg JM, Gomez GA, Verma S, Moussa EJ, Wu SK, Priya R, Hoffman BD, Grashoff C, Schwartz MA, and Yap AS (2014). Tension-sensitive actin assembly supports contractility at the epithelial zonula adherens. Current Biology 24, 1689–1699. [PubMed: 25065757]

Lei Q-Y, Zhang H, Zhao B, Zha Z-Y, Bai F, Pei X-H, Zhao S, Xiong Y, and Guan K-L (2008). TAZ promotes cell proliferation and epithelial-mesenchymal transition and is inhibited by the hippo pathway. Molecular and cellular biology 28, 2426–2436. [PubMed: 18227151]

Li D, Liu Y, Pei C, Zhang P, Pan L, Xiao J, Meng S, Yuan Z, and Bi X (2017). miR-285–Yki/Mask double-negative feedback loop mediates blood–brain barrier integrity in Drosophila. Proceedings of the National Academy of Sciences 114, E2365–E2374.

Li H, Handsaker B, Wysoker A, Fennell T, Ruan J, Homer N, Marth G, Abecasis G, and Durbin R (2009). The sequence alignment/map format and SAMtools. Bioinformatics 25, 2078–2079. [PubMed: 19505943]

Lin C, Yao E, Zhang K, Jiang X, Croll S, Thompson-Peer K, and Chuang P-T (2017). YAP is essential for mechanical force production and epithelial cell proliferation during lung branching morphogenesis. eLife 6, e21130. [PubMed: 28323616]

Lin HV, Rogulja A, and Cadigan KM (2004). Wingless eliminates ommatidia from the edge of the developing eye through activation of apoptosis. Development 131, 2409–2418. [PubMed: 15128670]

Liu R, Abreu-Blanco MT, Barry KC, Linardopoulou EV, Osborn GE, and Parkhurst SM (2009). Wash functions downstream of Rho and links linear and branched actin nucleation factors. Development 136, 2849–2860. [PubMed: 19633175]

Lucas EP, Khanal I, Gaspar P, Fletcher GC, Polesello C, Tapon N, and Thompson BJ (2013). The Hippo pathway polarizes the actin cytoskeleton during collective migration of Drosophila border cells. J Cell Biol, jcb. 201210073.

Maartens AP, Wellmann J, Wictome E, Klapholz B, Green H, and Brown NH (2016). Drosophila vinculin is more harmful when hyperactive than absent, and can circumvent integrin to form adhesion complexes. J Cell Sci 129, 4354–4365. [PubMed: 27737911]

Machado-Neto JA, Lazarini M, Favaro P, Franchi GC, Nowill AE, Saad STO, and Traina F (2014). ANKHD1, a novel component of the Hippo signaling pathway, promotes YAP1 activation and cell cycle progression in prostate cancer cells. Experimental Cell Research 324, 137–145. [PubMed: 24726915]

Malartre M (2016). Regulatory mechanisms of EGFR signalling during Drosophila eye development. Cellular and Molecular Life Sciences 73, 1825–1843. [PubMed: 26935860]

Matsui Y, and Lai Z-C (2013). Mutual regulation between Hippo signaling and actin cytoskeleton. Protein & cell 4, 904–910. [PubMed: 24248471]

McNeill H, and Reginensi A (2017). Lats1/2 regulate Yap/Taz to control nephron progenitor epithelialization and inhibit myofibroblast formation. Journal of the American Society of Nephrology 28, 852–861. [PubMed: 27647853]

McNeill H, Yang C-H, Brodsky M, Ungos J, and Simon MA (1997). mirror encodes a novel PBX-class homeoprotein that functions in the definition of the dorsal-ventral border in the Drosophila eye. Genes & development 11, 1073–1082. [PubMed: 9136934]

Miller DT, and Cagan RL (1998). Local induction of patterning and programmed cell death in the developing Drosophila retina. Development 125, 2327–2335. [PubMed: 9584131]

Misra JR, and Irvine KD (2018). The Hippo Signaling Network and Its Biological Functions. Annual Review of Genetics 52, 65–87.

Monserrate J, and Brachmann CB (2007). Identification of the death zone: a spatially restricted region for programmed cell death that sculpts the fly eye. Cell Death & Differentiation 14, 209–217. [PubMed: 16710366]

Murray MJ, Davidson CM, Hayward NM, and Brand AH (2006). The Fes/Fer non-receptor tyrosine kinase cooperates with Src42A to regulate dorsal closure in Drosophila. Development 133, 3063–3073. [PubMed: 16831834]

Nahm M, Lee M, Baek S-H, Yoon J-H, Kim H-H, Lee ZH, and Lee S (2006). Drosophila RhoGEF4 encodes a novel RhoA-specific guanine exchange factor that is highly expressed in the embryonic central nervous system. Gene 384, 139–144. [PubMed: 17011730]

Nakamura M, Verboon JM, and Parkhurst SM (2017). Prepatterning by RhoGEFs governs Rho GTPase spatiotemporal dynamics during wound repair. J Cell Biol 216, 3959–3969. [PubMed: 28923977]

Nishimura T, and Takeichi M (2008). Shroom3-mediated recruitment of Rho kinases to the apical cell junctions regulates epithelial and neuroepithelial planar remodeling. Development 135, 1493. [PubMed: 18339671]

Oh H, and Irvine KD (2008). In vivo regulation of Yorkie phosphorylation and localization. Development 135, 1081–1088. [PubMed: 18256197]

Oh H, and Irvine KD (2011). Cooperative regulation of growth by Yorkie and Mad through bantam. Developmental cell 20, 109–122. [PubMed: 21238929]

Opazo Saez A, Zhang W, Wu Y, Turner CE, Tang DD, and Gunst SJ (2004). Tension development during contractile stimulation of smooth muscle requires recruitment of paxillin and vinculin to the membrane. American Journal of Physiology-Cell Physiology 286, C433–C447. [PubMed: 14576084]

Peng HW, Slattery M, and Mann RS (2009). Transcription factor choice in the Hippo signaling pathway: homothorax and yorkie regulation of the microRNA bantam in the progenitor domain of the Drosophila eye imaginal disc. Genes & development 23, 2307–2319. [PubMed: 19762509]

Piedra J, Miravet S, Castaño J, Pálmer HG, Heisterkamp N, de Herreros AG, and Dunach M (2003). p120 Catenin-associated Fer and Fyn tyrosine kinases regulate β-catenin Tyr-142 phosphorylation and β-catenin-α-catenin Interaction. Molecular and cellular biology 23, 2287–2297. [PubMed: 12640114]

Polesello C, and Tapon N (2007). Salvador-warts-hippo signaling promotes Drosophila posterior follicle cell maturation downstream of notch. Current Biology 17, 1864–1870. [PubMed: 17964162]

Rauskolb C, Sun S, Sun G, Pan Y, and Irvine KD (2014). Cytoskeletal tension inhibits Hippo signaling through an Ajuba-Warts complex. Cell 158, 143–156. [PubMed: 24995985]

Ready DF, Hanson TE, and Benzer S (1976). Development of the Drosophila retina, a neurocrystalline lattice. Developmental biology 53, 217–240. [PubMed: 825400]

Reddy B, and Irvine KD (2013). Regulation of Hippo signaling by EGFR-MAPK signaling through Ajuba family proteins. Developmental cell 24, 459–471. [PubMed: 23484853]

Reginensi A, Enderle L, Gregorieff A, Johnson RL, Wrana JL, and McNeill H (2016). A critical role for NF2 and the Hippo pathway in branching morphogenesis. Nature communications 7, 12309.

Reginensi A, Hoshi M, Boualia SK, Bouchard M, Jain S, and McNeill H (2015). Yap and Taz are required for Ret-dependent urinary tract morphogenesis. Development 142, 2696–2703. [PubMed: 26243870]

Reginensi A, Scott RP, Gregorieff A, Bagherie-Lachidan M, Chung C, Lim D-S, Pawson T, Wrana J, and McNeill H (2013). Yap- and Cdc42-dependent nephrogenesis and morphogenesis during mouse kidney development. PLoS genetics 9, e1003380–e1003380. [PubMed: 23555292]

Ren F, Wang B, Yue T, Yun E-Y, Ip YT, and Jiang J (2010a). Hippo signaling regulates Drosophila intestine stem cell proliferation through multiple pathways. Proceedings of the National Academy of Sciences 107, 21064–21069.

Ren F, Zhang L, and Jiang J (2010b). Hippo signaling regulates Yorkie nuclear localization and activity through 14-3-3 dependent and independent mechanisms. Developmental biology 337, 303–312. [PubMed: 19900439]

Rosato R, Veltmaat JM, Groffen J, and Heisterkamp N (1998). Involvement of the tyrosine kinase fer in cell adhesion. Molecular and cellular biology 18, 5762–5770. [PubMed: 9742093]

Sansores-Garcia L, Atkins M, Moya IM, Shahmoradgoli M, Tao C, Mills GB, and Halder G (2013). Mask is required for the activity of the Hippo pathway effector Yki/YAP. Current Biology 23, 229–235. [PubMed: 23333314]

Sansores-Garcia L, Bossuyt W, Wada KI, Yonemura S, Tao C, Sasaki H, and Halder G (2011). Modulating F-actin organization induces organ growth by affecting the Hippo pathway. The EMBO journal 30, 2325–2335. [PubMed: 21556047]

Sarov M, Barz C, Jambor H, Hein MY, Schmied C, Suchold D, Stender B, Janosch S, Kj VV, and Krishnan R (2016). A genome-wide resource for the analysis of protein localisation in Drosophila. Elife 5, e12068. [PubMed: 26896675]

Schlegelmilch K, Mohseni M, Kirak O, Pruszak J, Rodriguez JR, Zhou D, Kreger BT, Vasioukhin V, Avruch J, and Brummelkamp TR (2011). Yap1 acts downstream of α-catenin to control epidermal proliferation. Cell 144, 782–795. [PubMed: 21376238]

Seiradake E, Jones EY, and Klein R (2016). Structural perspectives on axon guidance. Annual review of cell and developmental biology 32, 577–608.

Seo J, and Kim J (2018). Regulation of Hippo signaling by actin remodeling. BMB reports 51, 151. [PubMed: 29353600]

Seppa MJ, Johnson RI, Bao S, and Cagan RL (2008). Polychaetoid controls patterning by modulating adhesion in the Drosophila pupal retina. Developmental biology 318, 1–16. [PubMed: 18423436]

Sidor C, Borreguero-Munoz N, Fletcher GC, Elbediwy A, Guillermin O, and Thompson BJ (2019). Mask family proteins ANKHD1 and ANKRD17 regulate YAP nuclear import and stability. eLife 8, e48601. [PubMed: 31661072]

Sidor CM, Brain R, and Thompson BJ (2013). Mask proteins are cofactors of Yorkie/YAP in the Hippo pathway. Current Biology 23, 223–228. [PubMed: 23333315]

Silvis MR, Kreger BT, Lien W-H, Klezovitch O, Rudakova GM, Camargo FD, Lantz DM, Seykora JT, and Vasioukhin V (2011). α-catenin is a tumor suppressor that controls cell accumulation by regulating the localization and activity of the transcriptional coactivator Yap1. Sci Signal 4, ra33–ra33. [PubMed: 21610251]

Smith RK, Carroll PM, Allard JD, and Simon MA (2002). MASK, a large ankyrin repeat and KH domain-containing protein involved in Drosophila receptor tyrosine kinase signaling. Development 129, 71–82. [PubMed: 11782402]

Snigdha K, Gangwani KS, Lapalikar GV, Singh A, and Kango-Singh M (2019). Hippo Signaling in Cancer: Lessons From Drosophila Models. Front Cell Dev Biol 7, 85–85. [PubMed: 31231648]

Staley BK, and Irvine KD (2012). Hippo signaling in Drosophila: recent advances and insights. Developmental Dynamics 241, 3–15. [PubMed: 22174083]

Su T, Ludwig MZ, Xu J, and Fehon RG (2017). Kibra and merlin activate the hippo pathway spatially distinct from and independent of expanded. Developmental cell 40, 478–490. e473. [PubMed: 28292426]

Taguchi K, Ishiuchi T, and Takeichi M (2011). Mechanosensitive EPLIN-dependent remodeling of adherens junctions regulates epithelial reshaping. The Journal of cell biology 194, 643–656. [PubMed: 21844208]

Tapon N, Harvey KF, Bell DW, Wahrer DC, Schiripo TA, Haber DA, and Hariharan IK (2002). salvador Promotes both cell cycle exit and apoptosis in Drosophila and is mutated in human cancer cell lines. Cell 110, 467–478. [PubMed: 12202036]

Trapnell C, Roberts A, Goff L, Pertea G, Kim D, Kelley DR, Pimentel H, Salzberg SL, Rinn JL, and Pachter L (2012). Differential gene and transcript expression analysis of RNA-seq experiments with TopHat and Cufflinks. Nature protocols 7, 562–578. [PubMed: 22383036]

Trapnell C, Williams BA, Pertea G, Mortazavi A, Kwan G, Van Baren MJ, Salzberg SL, Wold BJ, and Pachter L (2010). Transcript assembly and quantification by RNA-Seq reveals unannotated transcripts and isoform switching during cell differentiation. Nature biotechnology 28, 511.

Verghese S, Bedi S, and Kango-Singh M (2012). Hippo signalling controls Dronc activity to regulate organ size in Drosophila. Cell death and differentiation 19, 1664. [PubMed: 22555454]

Wada K-I, Itoga K, Okano T, Yonemura S, and Sasaki H (2011). Hippo pathway regulation by cell morphology and stress fibers. Development 138, 3907–3914. [PubMed: 21831922]

Watt KI, Harvey KF, and Gregorevic P (2017). Regulation of tissue growth by the mammalian hippo signaling pathway. Frontiers in physiology 8, 942. [PubMed: 29225579]

White K, Grether M, Abrams J, Young L, Farrell K, and Steller H (1994). Genetic control of programmed cell death in Drosophila. Science 264, 677–683. [PubMed: 8171319]

Wittkorn E, Sarkar A, Garcia K, Kango-Singh M, and Singh A (2015). The Hippo pathway effector Yki downregulates Wg signaling to promote retinal differentiation in the Drosophila eye. Development 142, 2002–2013. [PubMed: 25977365]

Wolff T, and Ready D (1993). The development of Drosophila melanogaster. Cold Spring Harbor Laboratory Press, Plainview, 1277–1325.

Wolff T, and Ready DF (1991a). The beginning of pattern formation in the Drosophila compound eye: the morphogenetic furrow and the second mitotic wave. Development 113, 841–850. [PubMed: 1726564]

Wolff T, and Ready DF (1991b). Cell death in normal and rough eye mutants of Drosophila. Development 113, 825–839. [PubMed: 1821853]

Wu S, Huang J, Dong J, and Pan D (2003). hippo encodes a Ste-20 family protein kinase that restricts cell proliferation and promotes apoptosis in conjunction with salvador and warts. Cell 114, 445–456. [PubMed: 12941273]

Wu S, Liu Y, Zheng Y, Dong J, and Pan D (2008). The TEAD/TEF family protein Scalloped mediates transcriptional output of the Hippo growth-regulatory pathway. Developmental cell 14, 388–398. [PubMed: 18258486]

Xu J, Vanderzalm PJ, Ludwig M, Su T, Tokamov SA, and Fehon RG (2018). Yorkie functions at the cell cortex to promote myosin activation in a non-transcriptional manner. Developmental cell 46, 271–284. e275. [PubMed: 30032991]

Yao P.a., Li Y, Shen W, Xu X, Zhu W, Yang X, Cao J, and Xing C (2018). ANKHD1 silencing suppresses the proliferation, migration and invasion of CRC cells by inhibiting YAP1-induced activation of EMT. American journal of cancer research 8, 2311–2324. [PubMed: 30555746]

Yonemura S, Wada Y, Watanabe T, Nagafuchi A, and Shibata M (2010). α-Catenin as a tension transducer that induces adherens junction development. Nature cell biology 12, 533. [PubMed: 20453849]

Yu J, Poulton J, Huang Y-C, and Deng W-M (2008). The hippo pathway promotes Notch signaling in regulation of cell differentiation, proliferation, and oocyte polarity. PloS one 3, e1761–e1761. [PubMed: 18335037]

Yue T, Tian A, and Jiang J (2012). The cell adhesion molecule echinoid functions as a tumor suppressor and upstream regulator of the Hippo signaling pathway. Developmental cell 22, 255–267. [PubMed: 22280890]

Zerbino DR, Achuthan P, Akanni W, Amode MR, Barrell D, Bhai J, Billis K, Cummins C, Gall A, Girón CG, et al. (2018). Ensembl 2018. Nucleic acids research 46, D754–D761. [PubMed: 29155950]

Zhao B, Li L, Wang L, Wang C-Y, Yu J, and Guan K-L (2012). Cell detachment activates the Hippo pathway via cytoskeleton reorganization to induce anoikis. Genes & development 26, 54–68. [PubMed: 22215811]

Zhao B, Wei X, Li W, Udan RS, Yang Q, Kim J, Xie J, Ikenoue T, Yu J, and Li L (2007). Inactivation of YAP oncoprotein by the Hippo pathway is involved in cell contact inhibition and tissue growth control. Genes & development 21, 2747–2761. [PubMed: 17974916]

Zheng Y, and Pan D (2019). The hippo signaling pathway in development and disease. Developmental cell 50, 264–282. [PubMed: 31386861]

Zhou Z, Jiang H, Tu K, Yu W, Zhang J, Hu Z, Zhang H, Hao D, Huang P, and Wang J (2019). ANKHD1 is required for SMYD3 to promote tumor metastasis in hepatocellular carcinoma. Journal of Experimental & Clinical Cancer Research 38, 18.

Zhu M, Li X, Tian X, and Wu C (2015a). Mask loss-of-function rescues mitochondrial impairment and muscle degeneration of Drosophila pink1 and parkin mutants. Human molecular genetics 24, 3272–3285. [PubMed: 25743185]

Zhu Y, Li D, Wang Y, Pei C, Liu S, Zhang L, Yuan Z, and Zhang P (2015b). Brahma regulates the Hippo pathway activity through forming complex with Yki–Sd and regulating the transcription of Crumbs. Cellular signalling 27, 606–613. [PubMed: 25496831]

Manuscript Highlights:

- Mask functions within the context of Hippo signaling to regulate morphogenesis of the *Drosophila* pupal eye.
- Appropriate accumulation and distribution of Adherens Junctions requires Mask and Yki.
- Numerous genes associated with adhesion, the cytoskeleton, and tissue morphogenesis are responsive to Mask in the pupal eye.
- Correct expression of *FER* and *Vinc*, which are downstream of Mask, is essential for the accumulation of Adherens Junctions and hence pattern formation.

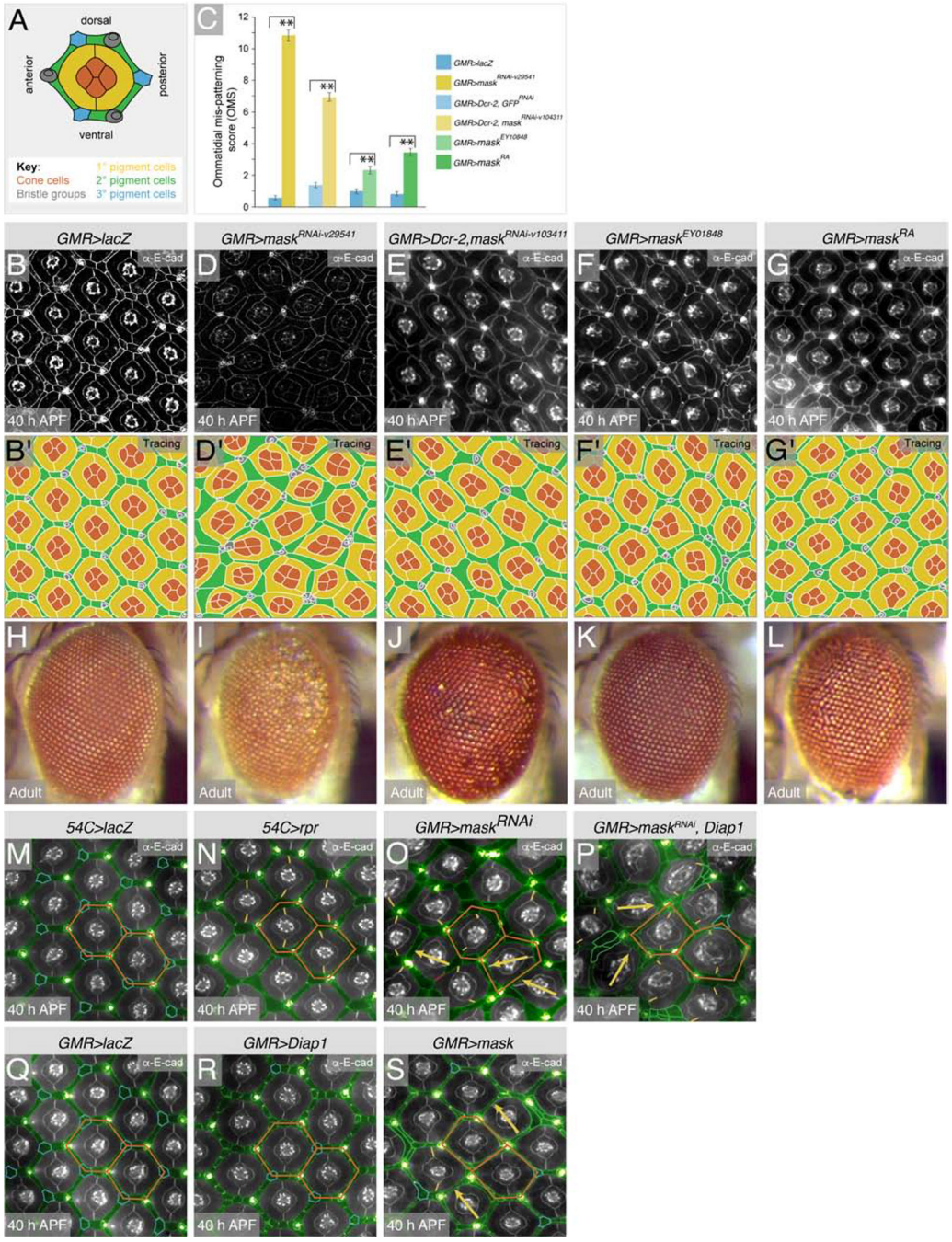

Figure 1: Mask is required for patterning of the *Drosophila* eye independent of lattice cell number.

(A) Cartoon of a single ommatidium and surrounding lattice cells at 40 h APF. (B) Small region of a control retina at 40 h APF expressing *lacZ*, which does not disturb patterning. (C) Histograms of mean OMS scores for the genotypes in panels (B) and (D)-(G), ** denote *p*-value < 0.01. Retinas with (D) $mask^{RNAi\text{-}v29541}$, (E) $mask^{RNAi\text{-}v103411}$, (F) $mask^{EY01848}$, or (G) $mask^{RA}$. (B') and (D')-(G') Tracings of images, with cone cells in orange, 1°s in yellow, lattice cells in green and bristle groups in grey. Confocal imaging settings were identical for panels (B) and (D). Images in (E-G) were generated with different imaging

settings. See Table S3A,B for analyses of patterning defects. Representative eyes of (H) *GMR>lacZ*, (I) *GMR>mask*$^{RNAi\text{-}v29541}$, (J) *GMR>mask*$^{RNAi\text{-}v103411}$, (K) *GMR>mask*^{EY01848} and (L) *GMR>mask* ^{RA} adults. Retinas at 40 h APF expressing (M) *lacZ* or (N) *rpr* with the lattice-specific *54C-Gal4* driver, and (O) *mask*$^{RNAi\text{-}v29541}$, (P) *mask*$^{RNAi\text{-}v29541}$ *and Diap1*, (Q) *lacZ* (R) *Diap1* and (S) *mask*^{EY01848} driven by *GMR-Gal4*. For (M)-(S) E-cad-detection was optimized during imaging to facilitate easier scoring of mis-patterning. 2 ommatidia are outlined (orange) to emphasize their shapes. Interommatidial cells are pseudo-colored green. Correctly-patterned 3°s are outlined in blue. Examples of grouped lattice cells are outlined in green and mis-oriented ommatidia indicated with yellow arrows. Abutting ommatidia are indicated with red lines. Yellow lines at 1°:1° boundaries emphasize relative size of 1° pairs.

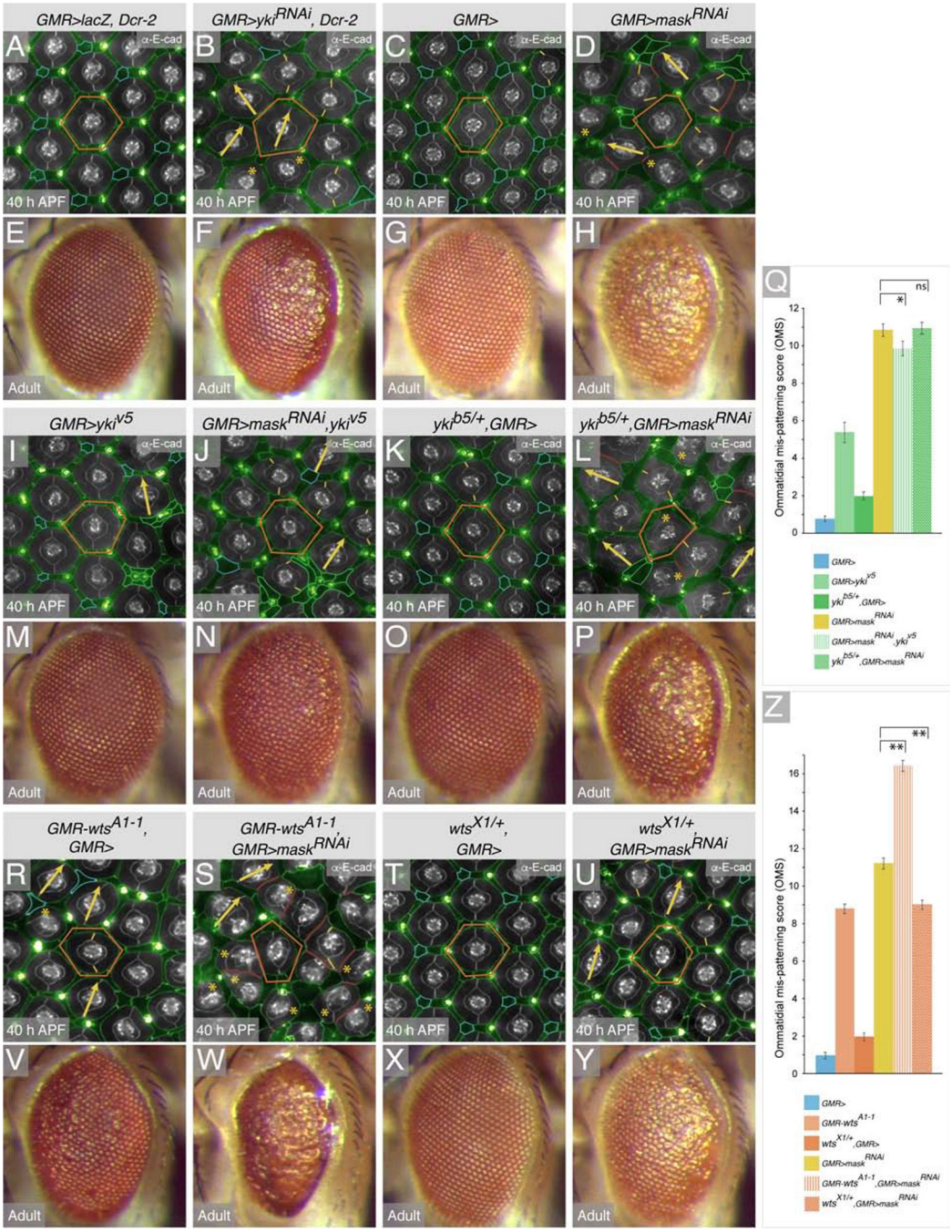

Figure 2: Yki and Wts are required for eye morphogenesis.

Smalls regions of retinas at 40 h APF expressing (A) *lacZ* and *Dcr-2*, or (B) yki^{RNAi} and *Dcr-2*, (C) heterozygous for *GMR-Gal4* or (D) expressing $mask^{RNAi\text{-}v2954}$ and (E)-(H) representative eyes of adults of these genotypes. See Table S3D for further analyses of mis-patterning. Retinas at 40 h APF expressing (I) ectopic *yki*, and (J) ectopic *yki* and $mask^{RNAi\text{-}v29541}$. (K) A retina heterozygous for *GMR-Gal4* and yki^{b5}, and (L) in addition with $mask^{RNAi\text{-}v29541}$ expression. (M)-(P) Representative eyes of adults of genotypes (I)-(L). (Q) Mean OMS analyses at 40 h APF, for indicated genotypes. See Table S3E for further

analyses of mis-patterning. (R) A retina heterozygous for *GMR-Gal4* and a *GMR-wts* transgene, and (S) in addition with $mask^{RNAi\text{-}v29541}$ expression. (T) A retina heterozygous for wts^{X1} and *GMR-Gal4* or (U) in addition $mask^{RNAi\text{-}v29541}$. (V)-(Y) Representative eyes of adults of genotypes (R)-(U). (Z) Mean OMS analyses at 40 h APF, for indicated genotypes. See Table S3F for further analyses of mis-patterning. For panels (Q) and (Z), given the goal of testing modification of patterning in $GMR{>}mask^{RNAi\text{-}v29541}$ retina when *yki* or *wts* expression was modified, significant changes in only these data are indicated. * denotes p-value < 0.1; ** denotes p-value < 0.01; ns = not significant. Abutting ommatidia are indicated with red lines; yellow * denote ommatidia missing 1°s; all other annotations as described in Figure 1. E-cad-imaging was optimized and images processed so that patterning defects could be scored.

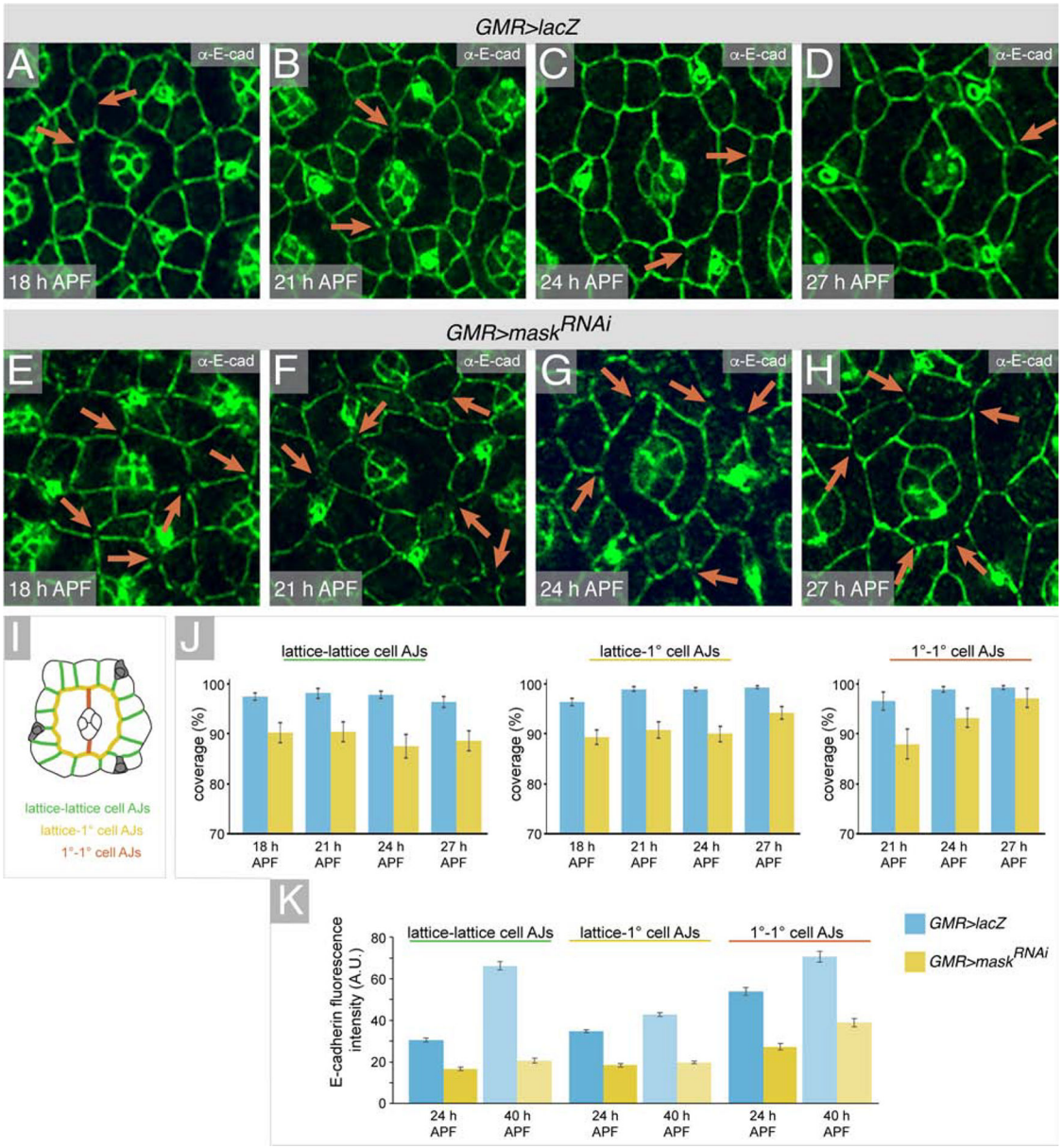

Figure 3: AJs are not correctly organized when *mask* is reduced.

GMR>lacZ ommatidia at (A) 18, (B) 21, (C) 24 and (D) 27 h APF and (E)-(H) *GMR>mask*$^{RNAi\text{-}v29541}$ ommatidia at analogous ages. Images (A)-(H) were gathered using identical confocal settings, but E-cad was enhanced in panels presented so that inconsistencies in AJ distribution can be observed. Orange arrows indicate examples of gaps in E-cad detection. (I) Cartoon of an ommatidium indicating the different AJs analyzed in (J), quantification of E-cad/AJ distribution in *GMR>lacZ* and *GMR>mask*$^{RNAi\text{-}v29541}$ retinas. For N and *p*-values see Table S4B. (K) Quantification of amount of E-cad at AJs in *GMR>lacZ* and *GMR> mask*$^{RNAi\text{-}v29541}$ retinas at 24 and 40 h APF. For N and *p*-values see Table S4C. In (J) and (K) all *p*-values were < 0.1 with the exception of the difference between E-cad coverage between 1° cells at 27 h APF (J). Error bars reflect standard error.

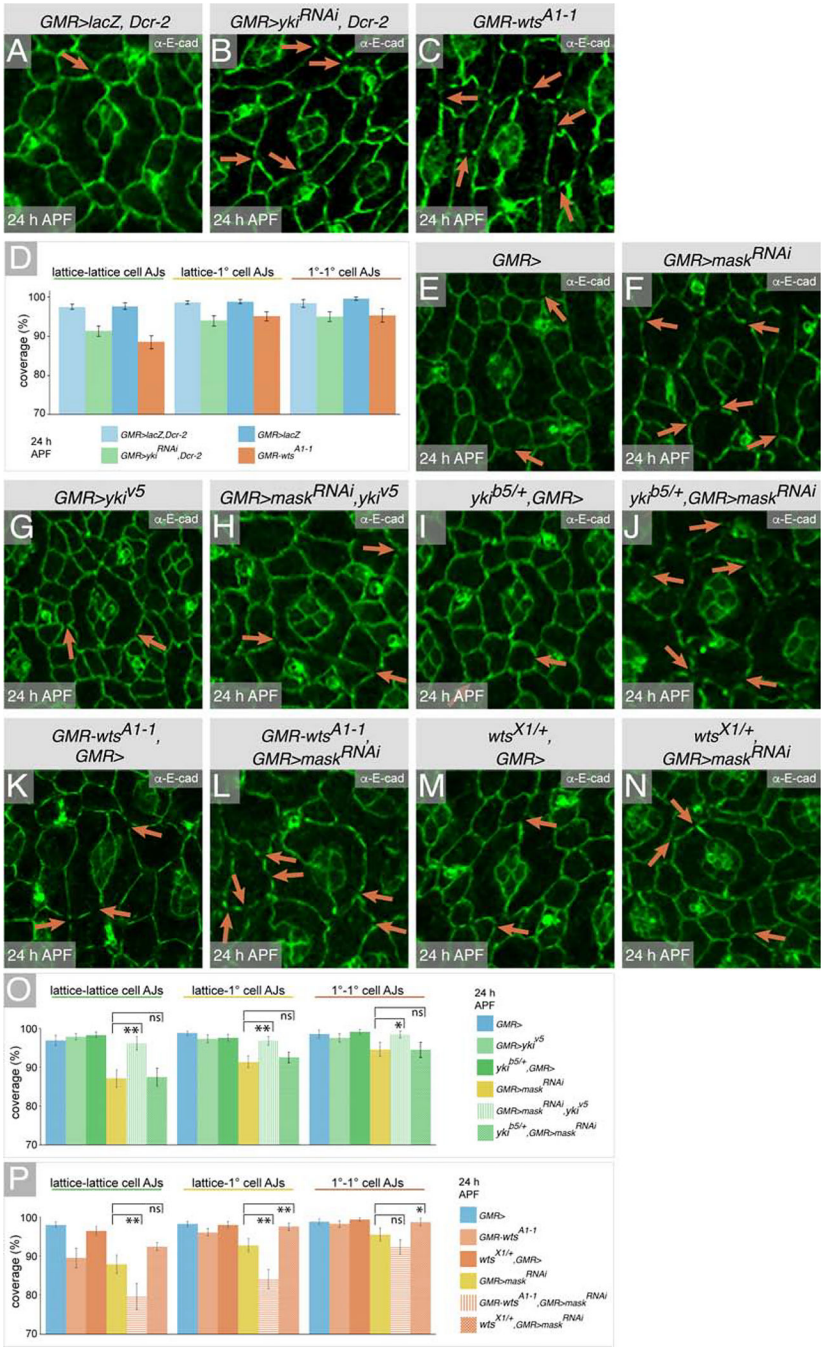

Figure 4: AJ result from compromised Hippo pathway activity.

Ommatidia at 24 h APF expressing (A) *lacZ* and *Dcr-2*, (B) *yki*^{RNAi} and *Dcr-2*, or (C) ectopic *wts* and (D) quantification of AJ distribution; all *p*-values were < 0.1. For N and *p*-values see Table S4D. Ommatidia at 24 h APF heterozygous for (E) *GMR-Gal4* or expressing (F) *mask*$^{RNAi\text{-}v29541}$, (G) *yki*, and (H) *yki* and *mask*$^{RNAi\text{-}v29541}$, heterozygous for (I) *GMR-Gal4* and *yki*^{b5}, or (J) in addition with *mask*$^{RNAi\text{-}v29541}$ expression, heterozygous for (K) *GMR-Gal4* and a *GMR-wts* transgene, and (L) in addition with *mask*$^{RNAi\text{-}v29541}$ expression, heterozygous for (M) *wts*^{X1} and *GMR-Gal4*, and (N) in addition

mask$^{RNAi\text{-}v29541}$. (O) Quantification of E-cad/AJ distribution for genotypes (E)-(J). For N and *p*-values see Table S4E. (P) Quantification of E-cad/AJ distribution for genotypes (E), (F),(K)-(N). For N and *p*-values see Table S4F. Given the goal of testing modification of AJ distribution by *yki* and *wts* in *GMR>mask*$^{RNAi\text{-}v29541}$ retinas, significant changes in only these data are indicated in O and P. * denotes *p*-value < 0.1; ** denote *p*-value < 0.05; ns = not significant. Error bars reflect standard error. E-cad was enhanced in all images presented so that inconsistencies in AJ distribution can be observed. Orange arrows indicate examples of gaps in E-cad detection.

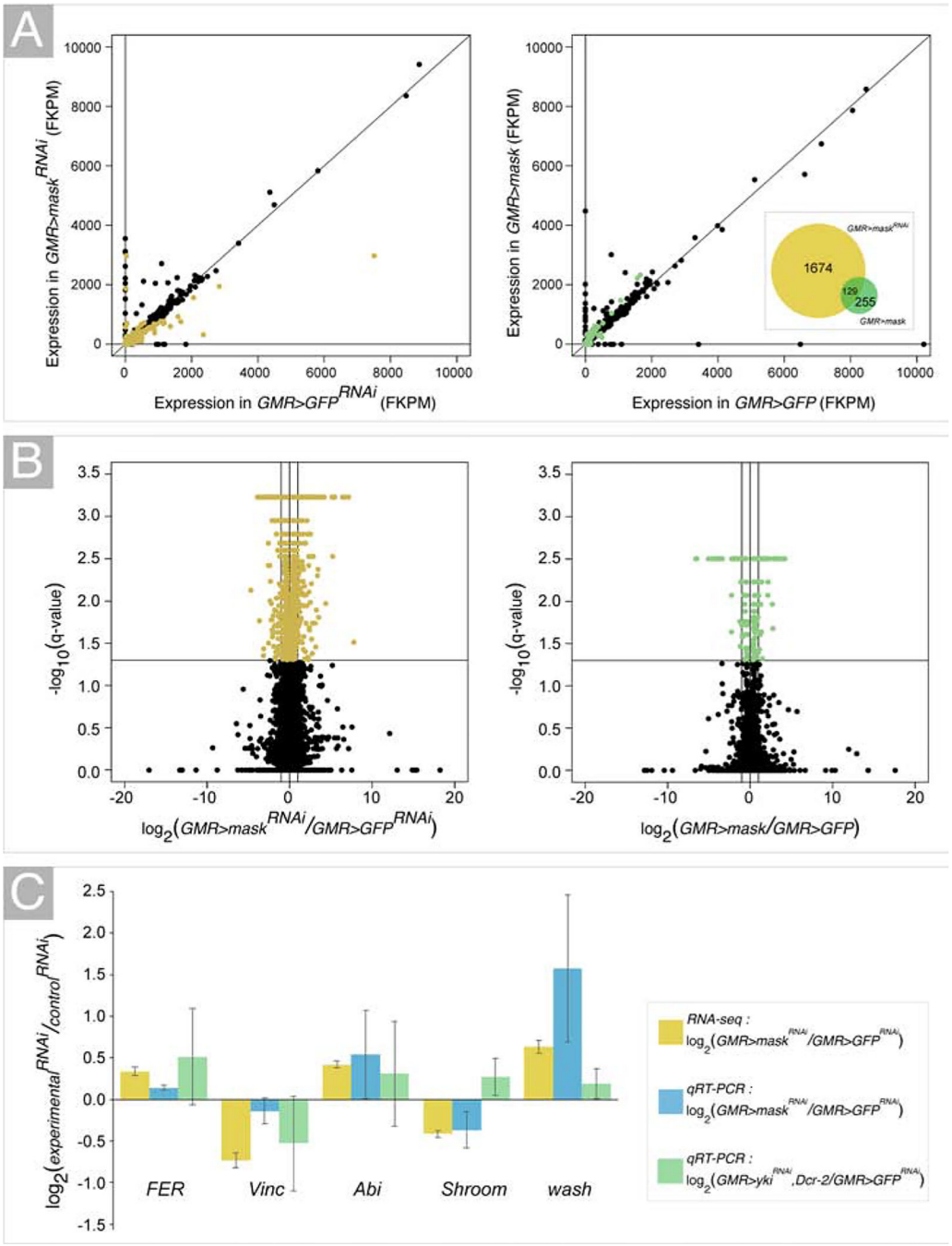

Figure 5: Analyses of transcriptional changes in retinas in response to Mask.

(A) Scatterplots of gene expression (FKPM = fragments per kilobase per million reads) in retinas at 24 h APF in which *mask* expression was reduced (left) or increased (right), in comparison to control retinas. Yellow and green points indicate loci that were significantly differentially expressed when *mask* was modified ($q < 0.05$). Expression of 1674 genes was modified in *GMR>mask*$^{RNAi\text{-}v29541}$ retinas and 255 in *GMR>mask* retinas, with 129 of these loci common to both data sets (see inset Venn diagram at right). (B) Volcano plots comparing significance ($-\log_{10}$ (q-value)) with the magnitude of expression change when

mask expression was reduced (left) or increased (right) compared to corresponding controls. A q-value of 0.05 corresponds to $-\log_{10}$ (q-value) of ~1.3 and all yellow or green points indicate differentially-expressed loci. (C) Plot of *FER*, *Vinc*, *Abi*, *Shroom*, and *wash* expression assessed with RNA-seq and qRT-PCR in *GMR>mask*$^{RNAi\text{-}v29541}$ or *GMR>yki*^{RNAi} retinas at 24 h APF. Error bars represent standard error.

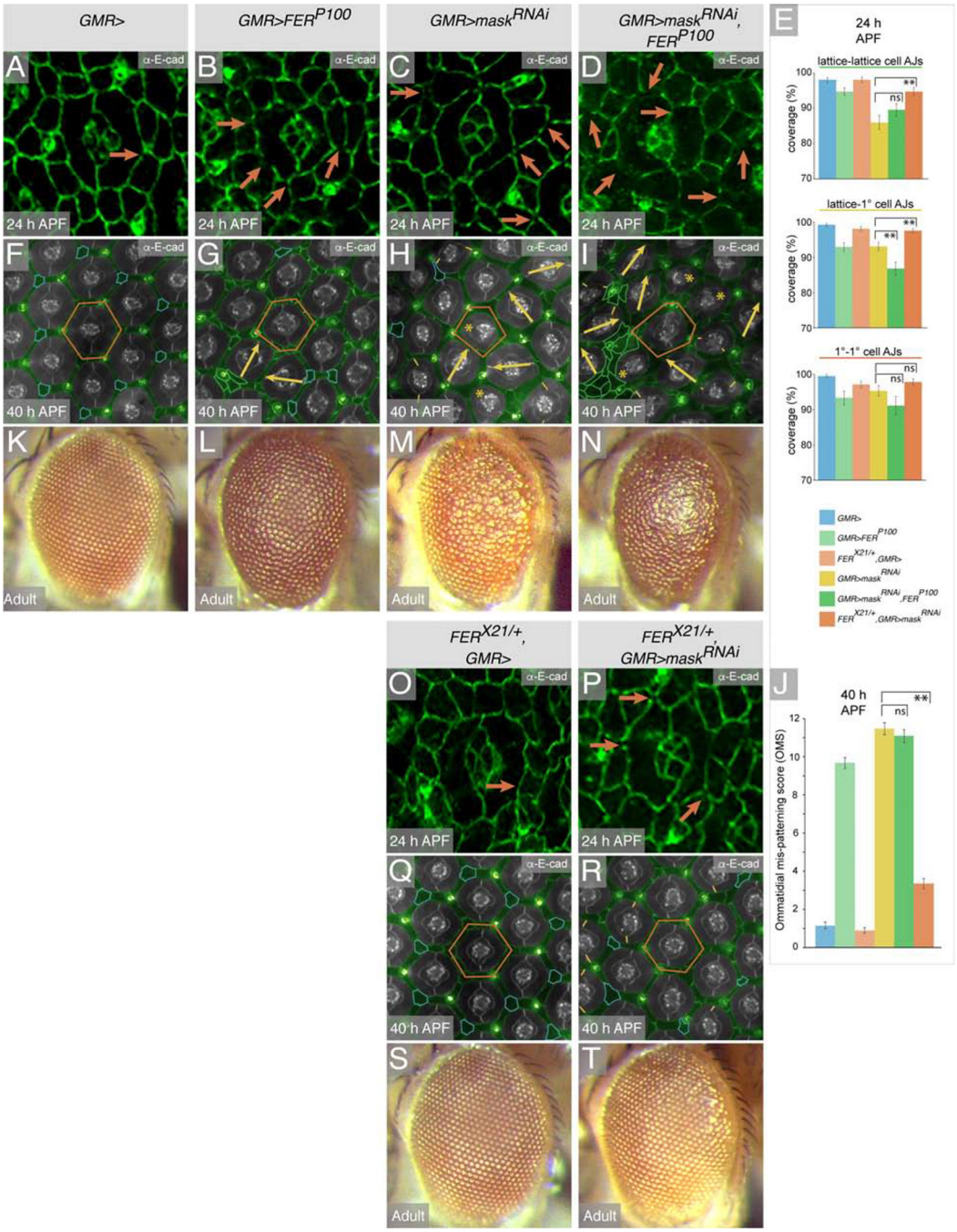

Figure 6: FER mediates the role of Mask in regulating adhesion.

Ommatidia at 24 h APF (A) heterozygous for *GMR-Gal4*, (B) with ectopic FER^{P100}, (C) $mask^{RNAi\text{-}v29541}$ or, (D) FER^{P100} and $mask^{RNAi\text{-}v29541}$. As before, tissue was imaged with identical confocal settings, but the images presented enhanced for better visualization of AJs. (E) Quantification of AJ (E-cad) distribution in retinas at 24 h APF. For N and *p*-values see Table S4G. (F)-(I) Retinas dissected at 40 h APF of genotypes (A)-(D). (J) Mean OMS values at 40 h APF, see Table S3H for detailed analyses. Given the goal of testing modification of $GMR{>}mask^{RNAi\text{-}v29541}$ by *FER*, significant changes in only these data are

indicated in (E) and (J); ** denotes *p*-value < 0.01; ns = not significant. Error bars reflect standard error. (K)-(N) Representative adult eyes of genotypes (A)-(D). (O) Ommatidia at 24 h APF heterozygous for *GMR-Gal4* and FER^{X21}, and (P) in addition with $mask^{RNAi\text{-}v29541}$. (Q)-(R) Retinas of these two genotypes dissected at 40 h APF and (S)-(T) representative adult eyes. All annotations are as described in Figures 1–3.

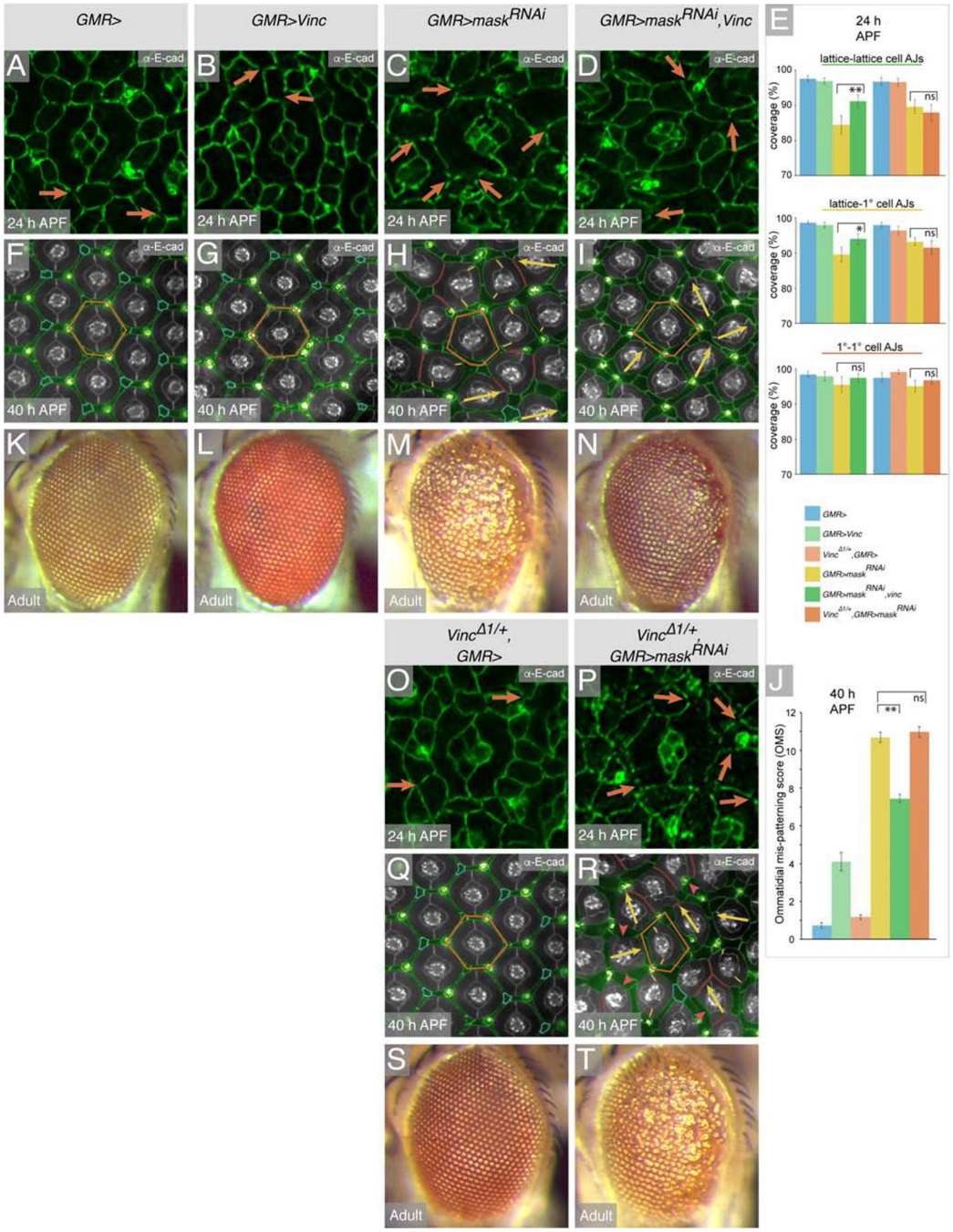

Figure 7: Vinculin modifies the mis-patterning generated by *mask*^{RNAi}.

Ommatidia at 24 h APF in retinas (A) heterozygous for *GMR-Gal4*, (B) with ectopic *Vinc*, (C) *mask*$^{RNAi\text{-}v29541}$, and (D) with ectopic *Vinc* and *mask*$^{RNAi\text{-}v29541}$. As before, eyes were imaged with identical confocal settings, but image panels enhanced for better visualization of AJs distribution. (E) AJ distribution at 24 h APF. For N and *p*-values see Table S4H. (F)-(I) Retinas dissected at 40 h APF of genotypes (A)-(D) and (J) mean OMS values at 40 h APF, see Table S3J for detailed analyses. Given the goal of testing modification of *GMR>mask*$^{RNAi\text{-}v29541}$ by *Vinc*, significant changes in only these data are indicated in (E)

and (J); * denotes *p*-value < 0.1; ** denotes *p*-value < 0.05; ns = not significant. Error bars reflect standard error. (K)-(N) representative adult eyes of genotypes (A)-(D). (O) Ommatidia at 24 h APF in retina heterozygous for *GMR-Gal4* and $Vinc^{\Delta 1}$, and (N) in addition $mask^{RNAi\text{-}v29541}$ and (Q)-(R) retinas of these two genotypes dissected at 40 h APF and (S)-(T) representative adult eyes. Annotations are as described in Figures 1–3.

KEY RESOURCES TABLE

Reagent or resource	**Source**	**Identifier**
Antibodies		
rat anti-E-cad (1:20)	Developmental Studies Hybridoma Bank	Cat#528120
mouse anti-Discs large (1:50)	Developmental Studies Hybridoma Bank	Cat#528203
rabbit anti-Dcp-1 (1:100)	Cell Signaling Technology	Cat#9578
rabbit anti-PH3 (1:200)	Millipore Sigma	Cat#06–570
chicken anti-GFP (1:20)	Abcam	Cat#13970
rabbit anti-Mask (1:500)	Smith et al., 2002	N/A
phalloidin (1:500)	Thermofisher Scientific	Cat#P3457
mouse anti-Lamin DMO (1:10)	Developmental Studies Hybridoma Bank	Cat#528336
Critical Commercial Assays		
ReliaPrep RNA Tissue Miniprep System	Promega Corporation	Cat#M3001
Experimental Models: *D.melanogaster*		
GMR-GAL4 *w[*]; P{w[+mC]=GAL4-ninaE.GMR}12*	Bloomington Drosophila Stock Center	BDSC:#1104
w^{1118} *w[1118]*	Bloomington Drosophila Stock Center	BDSC:#3605
Gal4–54C *y[1] w[*]; P{w[+m*]=GAL4}54C*	Bloomington Drosophila Stock Center	BDSC:#27328
mirror-Gal4 / TM6b *y[1] w[*]; wg[Sp-1]/CyO; P{w[+mW.hs]=GawB}mirr[DE]/TM3, Sb[1]*	Bloomington Drosophila Stock Center	From BDSC:#29650
ptc-Gal4 *w[*]; P{w[+mW.hs]=GawB}ptc[559.1]*	Bloomington Drosophila Stock Center	BDSC:#2017
$UAS\text{-}FER^{dsRNA}$; $UAS\text{-}FER^{dsRNA}$ *w[*]; P{w[+mC]=UAS-FER.dsRNA}SK-2; P{w[+mC]=UAS-FER.dsRNA}SK-3*	Bloomington Drosophila Stock Center	BDSC:#9366
$UAS\text{-}GFP^{dsRNA}$ *w[1118]; P{w[+mC]=UAS-GFP.dsRNA.R}142*	Bloomington Drosophila Stock Center	BDSC:#9330
$mask^{EY01848}$ *y[1] w[67c23]; P{w[+mC] y[+mDint2]=EPgy2}EY01848*	Bloomington Drosophila Stock Center	BDSC:#15378
$UAS\text{-}mask^{RA}$	Zhu et al., 2015a	N/A
$UAS\text{-}2XEGFP^{AH2}$ *w[*]; P{w[+mC]=UAS-2xEGFP}AH2*	Bloomington Drosophila Stock Center	BDSC:#6874
$UAS\text{-}yki^{V5.O}$ *w[*]; P{y[+t7.7] w[+mC]=UAS-yki.V5.O}attP2*	Bloomington Drosophila Stock Center	BDSC:#28819
UAS-FER.p100 *w[*]; P{w[+mC]=UAS-FER.p100}2; MKRS/TM6B, Tb[1]*	Bloomington Drosophila Stock Center	From BDSC:#9365
$UAS\text{-}shg^{R5}$ *w[*]; P{w[+mC]=UASp-shg.R}5*	Bloomington Drosophila Stock Center	BDSC:#58494
UAS-lacZ *w[1118]; P{w[+mC]=UAS-lacZ.NZ}20b*	Bloomington Drosophila Stock Center	BDSC:#3955

Reagent or resource	Source	Identifier
UAS-GFP *w[1118]; P{w[+mC]=UAS-GFP.nls}8*	Bloomington Drosophila Stock Center	BDSC:#4776
UAS-Diap1 *w[*]; P{w[+mC]=UAS-DIAP1.H}3*	Bloomington Drosophila Stock Center	BDSC:#6657
UAS-rpr *w[1118]; P{w[+mC]=UAS-rpr.C}14*	Bloomington Drosophila Stock Center	BDSC:#5824
UAS-Vinc RFP	Maartens et al., 2016	N/A
GMR-wts^{A1-1}	Tapon et al., 2002	N/A
wts^{X1}*,FRT82b / TM6b* *w[*]; wts[x1] P{ry[+t7.2]=neoFRT}82B/TM6B, Tb[1]*	Bloomington Drosophila Stock Center	BDSC:#44251
hsFLP^{12}*; FRT42D, hpo*^{KS240} */ CyO* *P{ry[+t7.2]=hsFLP}12, y[1] w[*];* *P{ry[+t7.2]=neoFRT}42D hpo[KS240]/CyO*	Bloomington Drosophila Stock Center	BDSC:#25085
ey-FLP^{N2} *; FRT42D, hpo*^{KC202} */ CyO, Kr-GFP* *y[d2] w[1118] P{ry[+t7.2]=ey-FLP.N}2;* *P{ry[+t7.2]=neoFRT}42D hpo[KC202]/CyO,* *P{w[+mC]=GAL4-Kr.C}DC3, P{w[+mC]=UAS-GFP.S65T}DC7*	Bloomington Drosophila Stock Center	BDSC:#25090
mer^{4}*,FRT19A / FM7i, Act-GFP* y[1] w[*] Mer[4] P{ry[+t7.2]=neoFRT}19A/FM7i, P{w[+mC]=ActGFP}JMR3	Bloomington Drosophila Stock Center	BDSC:#9104
ex^{e1}*, FRT40A / CyO* *w[*]; ex[e1] P{ry[+t7.2]=neoFRT}40A/CyO*	Bloomington Drosophila Stock Center	BDSC:#44249
FER^{X21} *w[*]; FER[X21], e[s] ca[1]*	Bloomington Drosophila Stock Center	BDSC:#9362
shg-tomato *y[1] w[*]; TI{TI}shg[mTomato]*	Bloomington Drosophila Stock Center	BDSC:#58789
lifeact-GFP *y[1] w[*]; P{y[+t*] w[+mC]=UAS-Lifeact-GFP}VIE-260B*	Bloomington Drosophila Stock Center	BDSC:#35544
sqh-GFP *w[1118]; P{w[+mC]=sqh-GFP.RLC}3*	Bloomington Drosophila Stock Center	BDSC:#57145
mask^{CC00924} *w[*]; P{w[+mC]=PTT-GC}mask[CC00924]*	Bloomington Drosophila Stock Center	BDSC:#51547
mask$^{5.8}$ */ TM6b*	Smith et al., 2002	N/A
mask$^{10.22}$ */ TM6b*	Smith et al., 2002	N/A
shg^{R69}*;TM2 / SM5-TM6b*	Godt and Tepass, 1998	N/A
yki^{B5}*,FRT42D / CyO-GFP*	Oh and Irvine, 2008	N/A
Vinc^{A1}	Klapholz et al., 2015	N/A
UAS-Ecad$^{RNAi\ B107A1}$	Seppa et al., 2008	N/A
GMR-Gal4, UAS-Dcr-2	Johnson et al., 2011	N/A
UAS-mask$^{RNAi\ GD14947}$	Vienna Drosophila Research Center	V29541
UAS-mask$^{RNAi\ GD9362}$	Vienna Drosophila Research Center	V33396
UAS-mask$^{RNAi\ kk100529}$	Vienna Drosophila Research Center	V103411
UAS-yki$^{RNAi\ kk109756}$	Vienna Drosophila Research Center	V104524

Reagent or resource	Source	Identifier
mask$^{sGFP\ fTRG486}$	Vienna Drosophila Research Center	V318123
yki$^{sGFP\ fTRG875}$	Vienna Drosophila Research Center	V318237
yki-YFP	Su et al, 2017	N/A
Software and Algorithms		
Galaxy	Afgan et al., 2018	https://usegalaxy.org
Ensembl	Zerbino et al., 2018	https://useast.ensembl.org/index.html
Flagstat	Li et al., 2009	https://www.htslib.org/doc/samtools-flagstat.html
FastQC	Andrews, 2010	https://www.bioinformatics.babraham.ac.uk/projects/fastqc/
Bowtie2	Langmead and Salzberg, 2012	http://bowtie-bio.sourceforge.net/bowtie2/index.shtml
Cufflinks	Trapnell et al., 2010	https://www.genepattern.org/modules/docs/Cufflinks
Cuffdiff	Trapnell et al., 2012	https://www.genepattern.org/modules/docs/Cuffdiff/7
The Gene Ontology Consortium	Alliance of Genome Resources	http://geneontology.org/
R Statistical Software	CRAN, 2018	https://www.r-project.org/